Leukemia www.nature.com/leu

ARTICLE



ACUTE MYELOID LEUKEMIA

Anagrelide and idarubicin combination induces GSDMEmediated pyroptosis as a potential therapy for high-PDE3A acute myeloid leukemia

© The Author(s), under exclusive licence to Springer Nature Limited 2024

Acute myeloid leukemia (AML) is an invasive hematopoietic malignancy requiring novel treatment strategies. In this study, we identified phosphodiesterase 3 A (PDE3A) as a potential new target for drug repositioning in AML. PDE3A was preferentially overexpressed in AML cells than in normal cells, and high expression of PDE3A was correlated with lower event-free survival (EFS) in de novo AML patients. The PDE3A inhibitor anagrelide (ANA) profoundly suppresses the proliferation of high PDE3A-expressing AML cells while exhibiting minimal impact on those with low PDE3A expression. Moreover, synergistic effect of ANA with other chemotherapeutic drugs in high PDE3A expression AML cells was observed. The ANA-idarubicin (IDA) combination showed the most remarkable synergistic effect among all ANA-chemotherapeutic drugs commonly used in AML cell line models. Mechanistically, the synergy between ANA and IDA inhibited the survival of PDE3A^{high} AML cell lines through pyroptosis. This mechanism was initiated by GSDME cleavage triggered by caspase-3 activation. In vivo combination treatment of leukemic animals with high PDE3A expression significantly reduced leukemia burden and prolonged survival time compared with single-drug and vehicle control treatments. Our findings suggest that combined ANA and IDA treatment is an innovative and promising therapeutic strategy for AML patients with high PDE3A expression.

Leukemia; https://doi.org/10.1038/s41375-024-02437-x

INTRODUCTION

Acute myeloid leukemia (AML) is a clinically aggressive and heterogeneous hematologic neoplasm characterized by acquired genetic abnormalities [1]. Current treatments for AML are limited, and the overall outcome of AML remains poor; only approximately 40% of younger patients (< 60 years) achieved long-term survival [2]; pediatric AML patients enrolled in clinical trials demonstrated a 70% survival rate [3], significantly lower than the 85–90% survival observed in young adults and children treated for acute lymphoblastic leukemia (ALL) [4]. The imperative task involves the identification of novel molecular targets and therapeutic strategies to ameliorate the overall survival rate of individuals afflicted by AML.

Platelets interact intricately with malignant cells, including leukemic blasts, which play pivotal roles in cancer progression, metastasis, and angiogenesis via diverse mechanisms. The platelet inhibitor clopidogrel significantly reduces tumor growth in an

orthotopic pancreatic tumor mouse model. The release of plateletderived microparticles promotes the transmission of numerous bioactive compounds to cancer cells upon internalization, contributing to the development of chemoresistance in AML [5-8]. Phosphodiesterase 3 (PDE3) is a member of the phosphodiesterase superfamily and comprises two subtypes: phosphodiesterase 3 A (PDE3A) and phosphodiesterase 3B. PDE3A is an extensively characterized cyclic nucleotide phosphodiesterase that catalyzes the hydrolysis of cyclic adenosine monophosphate (cAMP) and cyclic quanosine monophosphate (cGMP), orchestrating numerous vital intracellular signal transduction pathways and cellular processes [9-12]. PDE3A is predominantly expressed in vascular smooth muscles, platelets, oocytes, and the heart and plays a pivotal role in platelet aggregation and oocyte maturation [10]. Recent studies have reported the cAMP- and cGMPindependent functions of PDE3A. These studies have demonstrated that PDE3A is upregulated in several solid tumors and is

¹Department of Pediatric Hematology and Oncology, Children's Hospital of Soochow University, Suzhou 215000, China. ²Institution of Pediatric Research, Children's Hospital of Soochow University, Suzhou 215000, China. ³Department of Pediatric Surgery, Children's Hospital of Soochow University, Suzhou 215000, China. ⁴State Key Laboratory of Common Mechanism Research for Major Diseases and Key Laboratory of Synthetic Biology Regulatory Elements, Suzhou Institute of Systems Medicine, Chinese Academy of Medical Sciences & Peking Union Medical College, Suzhou 215123 Jiangsu, China. ⁵Department of Transfusion Medicine, Children's Hospital of Soochow University, Suzhou 215000, China. ⁶Jiangsu Pediatric Hematology & Oncology Center, Jiangsu, China. ⁷These authors contributed equally: Chenwei Yang, Yixin Hu, Li Gao, Zhiheng Li. ^{Se}email: yuanyuan.tian18@yahoo.com; hesd@ism.pumc.edu.cn; lingjing@suda.edu.cn; hushaoyan@suda.edu.cn

Received: 5 January 2024 Revised: 9 September 2024 Accepted: 7 October 2024

Published online: 15 October 2024

correlated with a poor prognosis [13–15]. The involvement of PDE3A in activating inflammatory pathways contributing to cancer cell stemness has been elucidated through the suppression of the cAMP/PKA pathway [13]. However, the precise expression pattern and functional implications of PDE3A in AML remain unclear.

The PDE3A inhibitor anagrelide (ANA) is an antithrombotic and platelet-reducing agent marketed for the treatment of thrombocythemia associated with myeloproliferative diseases. ANA therapy reduces the amount of circulating platelets by concurrently curtailing megakaryocyte hyperproliferation and differentiation processes [16, 17]. ANA treatment also suppresses cancer cell proliferation through apoptosis and cell cycle arrest, and its efficacy depends on the protein levels of PDE3A and SLFN12 [10, 18-20]. Similarly, the PDE3A inhibitor 6-(4-(diethylamino)-3nitrophenyl)-5-methyl-4,5-dihydropyridazin-3(2H)-one promotes cancer cell death by stabilizing the PDE3A-SLFN12 interaction [21-23]. The PDE3A inhibitor female sex hormone 17β-estradiol (E2) instigates cancer cell apoptosis by facilitating the interaction between PDE3A and SLFN12 within cells [24]. The PDE3A inhibitor, the indole alkaloid natural product nauclefine, elicits PDE3A-SLFN12-dependent apoptosis in tumor cells without inhibiting the enzymatic activity of PDE3A [25]. The PDE3A inhibitor, zardaverine (ZARD), selectively inhibited the growth of specific cancer cell lines [10]. These findings underscore the multifaceted role of PDE3A inhibitors in influencing cancer cell fate and highlight their potential therapeutic applications. However, the precise anticancer effects of PDE3A inhibitors on AML need to be elucidated further.

In the present study, we aimed to investigate the relationship between PDE3A expression and AML prognosis and to explore the feasibility and mechanism of PDE3A inhibition as a potential anti-leukemia treatment. We also aimed to identify novel synergistic strategies for AML treatment by combining PDE3A inhibitors with chemotherapeutic agents.

METHODS

Patients

Children aged <15 years with de novo AML, based on the World Health Organization (WHO) criteria, participated in this observational study. Bone marrow specimens were collected at the diagnosis stage and tested for morphology, immunotype, karyotype, DNA mutations, and genetic aberrations. Data on the RNA sequencing results of all patients were available. Details are available in the Supplemental Methods.

In vivo murine model

All animal experiments were conducted in compliance with the animal care guidelines approved by the Institutional Laboratory Animal Care and Use Committee of Soochow University. Five- to six-week-old NSG mice were purchased from Shanghai Model Organisms Center, Inc. Details are available in the Supplemental Methods.

Statistical analysis

Cell culture experiments were performed in at least three independent experiments for each cell line. Unless otherwise noted, the results were expressed as the mean ± standard deviation and were analyzed using a paired or unpaired t-test. Multiple groups were analyzed using a one-way analysis of variance. The correlations between continuous variables were calculated using Pearson correlation coefficients. Survival was estimated using the Kaplan-Meier method and compared using the log-rank test. Statistical significance was set at a P-value of <0.05 in all experiments. Data were analyzed and plotted using GraphPad Prism 8 software.

RESULTS

PDE3A overexpression in AML as a predictor of poor prognosis

To explore the potential role of PDE3A in AML, we analyzed its expression levels in 12 AML patients and 6 healthy donors; PDE3A

was expressed at a significantly higher level in bone marrow mononuclear cells (BMMNCs) from AML patients than in BMMNCs from healthy donors, at both the protein and messenger RNA (mRNA) levels (Fig. 1A, B). The clinical characteristics of patients with AML whose PDE3A protein levels are shown in Fig. 1A are presented in Table 1. These results showed that PDE3A was markedly overexpressed in AML cells and were validated by examining PDE3A expression levels in BMMNCs from AML patients and healthy donors using TCGA LAML database, and further confirmed through analysis with GEPIA (Fig. 1C).

To investigate the relationship between PDE3A expression and the patients' survival time, the correlation between PDE3A expression and prognosis of AML patients was subsequently investigated in 148 pediatric AML patients recruited in this retrospective study from October 2013 to September 2022 in our center. The baseline characteristics of patients are shown in Table 2. The transcriptomic expression level of PDE3A in newly diagnosed bone marrow samples was determined according to the results of RNA Sequencing. The patients were divided into two groups based on the 25th quartile of PDE3A expression: PDE3A high group (n = 111) and PDE3A low group (n = 37) (Fig. 1D). Results showed that AML patients in the PDE3A high group had significantly lower event-free survival (EFS) (Fig. 1E) compared with patients in the PDE3A low group. No significant difference was found in the overall survival (OS) between the two groups, but an obvious tendency toward lower OS was observed in patients with higher PDE3A expression (Fig. 1F). The results from the GEO database (GSE37642) analyzed via R2 indicated that AML patients with higher PDE3A expression exhibited lower OS than those with lower PDE3A expression (Fig. 1G). The patients were categorized based on the best truncation value (expression cut-off value: 133.6) of PDE3A expression. We also analyzed TCGA-LAML database using the GEPIA platform and stratified patients based on the median and 25th quartile. We observed that AML patients with a high expression of PDE3A had shorter OS than those with low expression of PDE3A; although a clear trend was evident, statistical significance was not achieved (Supplementary Fig. 1). PDE3A exhibits low expression levels in specific fusions of AML, including CBFB-MYH11 and other KMT2A rearrangements (except KMT2A-MLLT3 and KMT2A-MLLT11) (Fig. 1H, Table 2). These findings indicated that PDE3A can serve as a valuable biomarker for the diagnosis and prognosis of AML.

Overall, these observations revealed that PDE3A is overexpressed in AML, and high expression of PDE3A was closely related to poor prognosis in patients with AML.

PDE3A inhibitor ANA inhibiting the PDE3A high expressing AML cells in vitro and in vivo

To ascertain the anti-leukemia function of the PDE3A inhibitors, we investigated the PDE3A expression of AML cell lines from the CCLE database and found that PDE3A was highly expressed in HEL and MOLM-16 (Fig. 2A). To confirm this, we employed reverse transcription polymerase chain reaction (RT-PCR) and western blotting to explore the disparities in PDE3A expression across leukemic cell lines. Among these cell lines, HEL and MOLM-16 exhibited markedly elevated levels of PDE3A expression, surpassing those of the other cell lines both at the protein and transcriptional levels (Fig. 2B, C), which were selected as representative high-PDE3A-expressing models of AML for subsequent investigations. PDE3A inhibitor anagrelide (ANA) specifically inhibited the HEL and MOLM-16 growth in a concentrationdependent manner after 72 h of treatment. The half-maximal inhibitory concentrations (IC₅₀) (0.8 μM and 1.3 μM, respectively) of ANA were observed in HEL and MOLM-16 cells. Notably, ANA had no inhibitory effects on other AML cell lines that expressed low levels of PDE3A (Fig. 2D). The PDE3A inhibitors DNMDP, nauclefine, zardaverine, and E2 significantly reduced proliferation in HEL and MOLM-16 cells, while showing no inhibitory effects on

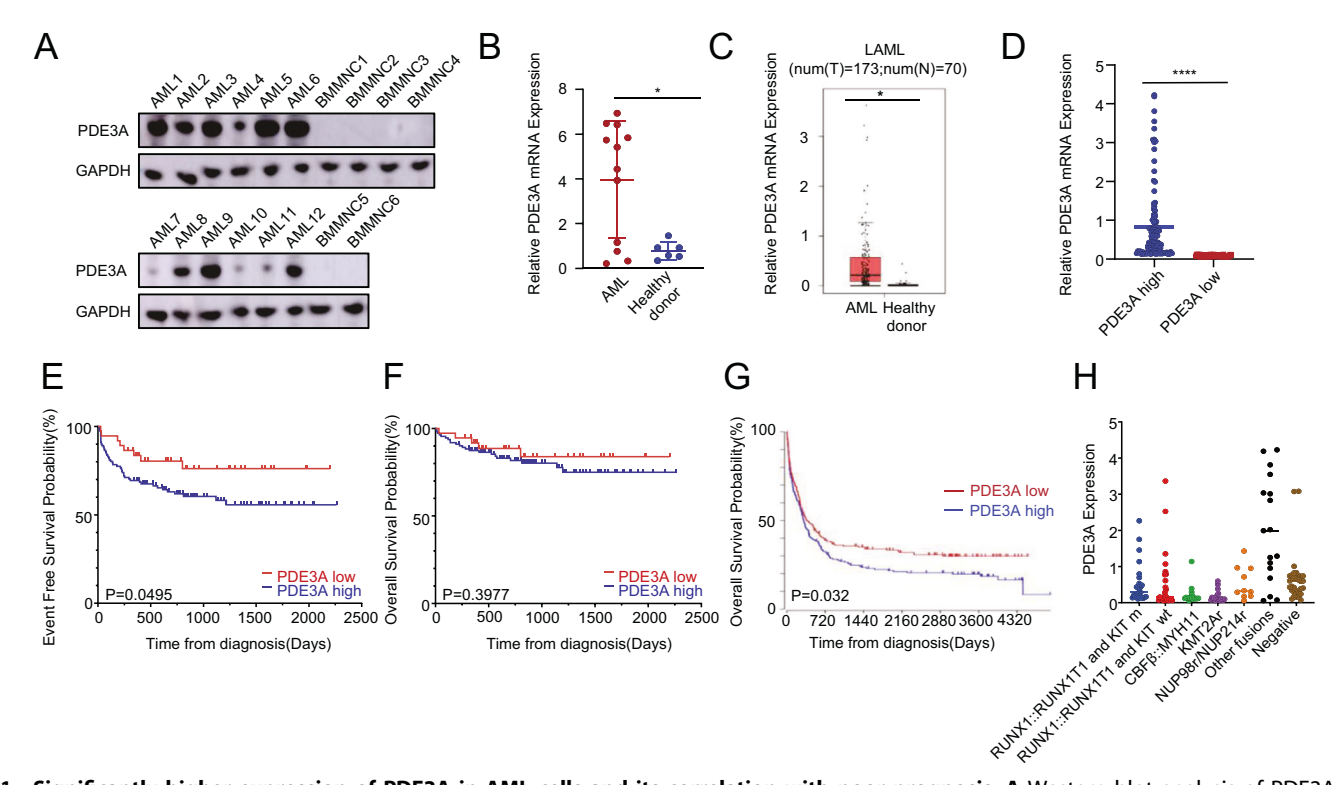


Fig. 1 Significantly higher expression of PDE3A in AML cells and its correlation with poor prognosis. A Western blot analysis of PDE3A protein levels in primary BMMNCs from patients with AML (n=12) and healthy donors (n=6) from the Children's Hospital of Soochow University and normalized to that of GAPDH. **B** Relative mRNA expression of PDE3A in primary BMMNCs from AML patients (n=12) and BMMNCs from healthy donors (n=6) in the Children's Hospital of Soochow University quantified using qRT-PCR and normalized to that of GAPDH. **C** Box plot of PDE3A expression in TCGA data set, comparing AML cell lines (n=173) and BMMNCs from healthy donors (n=70). **D** RNA sequencing analysis of patients divided into two groups based on the 25th quartile PDE3A expression: PDE3A^{high} group (n=111) and PDE3A^{low} group (n=37). EFS **E** and OS **F** of AML patients from the Children's Hospital of Soochow University stratified according to PDE3A expression status. **G** OS of AML patients in the R2 data set stratified according to PDE3A expression status. **H** Fusion gene expression of patients. Survival curves were analyzed using the Kaplan–Meier method, and *P*-values were determined using the log-rank (Mantel–Cox) test. Differences were compared using the two-tailed Student's *t*-test, and multiple groups were analyzed using the one-way analysis of variance. The data are expressed as the mean \pm SD (n=3). *P < 0.05, **P < 0.01, ****P < 0.001, ****P < 0.0001, NS not significant.

other AML cell lines exhibiting low PDE3A expression (Fig. 2E–H). We focused on examining the efficacy of ANA, a commercially available pharmaceutical, in our subsequent studies. Furthermore, to verify the anti-leukemia function of ANA in high PDE3A-expressing AML cells, primary cells from AML patients were divided into two groups according to the median PDE3A expression at the protein and transcriptional levels: PDE3A high group (n=6) and PDE3A low group (n=6); both groups were treated with 5 μ M ANA for 72 h. Consistent with the findings in AML cell lines, ANA drastically inhibited the proliferation of primary cells in the PDE3A high group and did not exert inhibitory effects on primary cells in the PDE3A low group (Fig. 2I).

To investigate the role of ANA in AML, the IC₅₀ of ANA was used for the treatment of HEL and MOLM-16 cells in our subsequent experiments. ANA inhibited the colony-forming ability (Fig. 3A) and interrupted the cell cycle by G1 arrest (Fig. 3B) in HEL and MOLM-16 cells, whereas cell apoptosis was hardly affected (Fig. 3C). Consistent with these results, the expression of cell cycle-related proteins including CyclinD1, CDK4, C-myc, CDK2, and CDK6 was significantly downregulated at the protein level in a time-dependent manner after ANA treatment in HEL and MOLM-16 cells compared with the control group. The G1 phase checkpoint-related proteins including P53, P27, and P21 were significantly upregulated at the protein level in a time-dependent manner after ANA treatment in HEL and MOLM-16 cells compared with the control group (Fig. 3D).

To evaluate the anti-leukemic activity of ANA in vivo, we developed a xenograft model of human AML by injecting 2 million

luciferase-overexpressing HEL cells into the tail vein of NSG mice (Fig. 3E). Fourteen days after leukemia cell implantation, the mice were treated daily with vehicle treatment or 5 mg/kg [19] ANA by gavage for 14 days. The in vivo imaging assay indicated that ANA treatment reduced the leukemia burden compared with vehicle treatment (Fig. 3F). Moreover, the anti-leukemia effects of ANA significantly prolonged the survival time compared with that following the vehicle treatment (Fig. 3G).

These results indicate that PDE3A inhibitors can suppress the proliferation of high PDE3A-expressing AML cell lines. ANA treatment inhibited colony-forming capacity, interrupted the cell cycle by G1 arrest, and inhibited leukemogenesis in a mouse xenograft model, and exerted an anti-leukemia effect on high PDE3A-expressing AML cells in vivo and in vitro.

Targeting PDE3A to downregulate the MAPK signaling pathway in high PDE3A-expressing AML cell lines

To further elucidate the mechanism underlying the anti-leukemia function of ANA, we performed RNA sequencing analysis of HEL cells and mRNA expression clustering, and plotted maps were created to identify the presence of differentially expressed genes (DEGs). Overall, treatment with ANA for 72 h resulted in dynamic alterations in transcription, with 146 upregulated and 197 downregulated genes (adjusted P < 0.05, absolute value \log_2 -Fold-change>0.5) (Fig. 4A). Kyoto Encyclopedia of Genes and Genomes (KEGG) analysis showed that categories related to "focal adhesion," "apelin signaling pathway," "MAPK signaling pathway," and "PPAR signaling pathway" were highly enriched (Fig. 4B).

Table 1. Characteristics of the patients included in Fig. 1A.

AML1 M3 14 M 123 2.88 317 AML2 M3 8 M 100 83.8 27 AML3 Unclassifiable 4 M 96 2.4 66 AML4 Unclassifiable 1 M 102 26 50 AML5 M5 2 F 96 123 274 AML6 M5 14 M 86 259 116 AML7 M4 12 M 98 20.5 17 AML8 M2 10 M 86 4.19 51 AML9 M5 10 F 97 2.2 191 AML10 M4 5 M 86 27.83 25 AML11 M4 7 M 106 25.04 145 ID Gene fusion ELT3-ITD 46,XY 45,XY+(15,17),(q24,q21) AML2 PML/RARA FLT3-ITD </th <th>ID</th> <th>FAB</th> <th>Age (year)</th> <th>Sex</th> <th>HB (g/L)</th> <th>WBC (×10⁹/L)</th> <th>PLT (×10⁹/L)</th>	ID	FAB	Age (year)	Sex	HB (g/L)	WBC (×10 ⁹ /L)	PLT (×10 ⁹ /L)	
AML3 Unclassifiable 4 M 96 2.4 66 AML4 Unclassifiable 1 M 102 26 50 AML5 M5 2 F 96 123 274 AML6 M5 14 M 86 259 116 AML7 M4 12 M 98 20.5 17 AML8 M2 10 M 86 4.19 51 AML8 M2 10 F 97 2.2 191 AML10 M4 5 M 86 27.83 25 AML11 M4 7 M 107 92.92 36 AML12 M2 7 M 106 25.04 145 ID Gene fusion Gene mutation Cytogenetics AML1 PML/RARA FLT3-ITD 46,XY(15,17),(q24,q22) AML2 PML/RARA FLT3-ITD 45,X-Y,t(8,21) (q22,q22)[11]/46,XY(5) <th>AML1</th> <th>M3</th> <th>14</th> <th>М</th> <th>123</th> <th>2.88</th> <th>317</th>	AML1	M3	14	М	123	2.88	317	
AML4 Unclassifiable 1 M 102 26 50 AML5 M5 2 F 96 123 274 AML6 M5 14 M 86 259 116 AML7 M4 12 M 98 20.5 17 AML8 M2 10 M 86 4.19 51 AML9 M5 10 F 97 2.2 191 AML10 M4 5 M 86 27.83 25 AML11 M4 7 M 107 92.92 36 AML12 M2 7 M 106 25.04 145 ID Gene fusion FLT3-ITD 46,XY 46,XY 46,XY AML1 PML/RARA FLT3-ITD 46,XY 46,XY 46,XY 46,XY AML3 RUNX/RUNXIT1 NRAS 46,XY 46,XY 46,XY 46,XY 46,XY 46,XY	AML2	M3	8	M	100	83.8	27	
AML5 M5 2 F 96 123 274 AML6 M5 14 M 86 259 116 AML7 M4 12 M 98 20.5 17 AML8 M2 10 M 86 4.19 51 AML9 M5 10 F 97 2.2 191 AML10 M4 5 M 86 27.83 25 AML11 M4 7 M 106 25.04 145 AML11 M4 7 M 106 25.04 145 AML1 PML/RARA 7 M 106 25.04 145 AML1 PML/RARA FLT3-ITD 46,XY 46,XY 46,XY AML3 RUNX/RUNX1T1 NRAS, KIT, IDH2 45,X-Yt(8,21) (q22,q22)[11]/46,XY(6] 46,XY(5)[1](q22,q22)[11]/46,XY(6] AML4 NPMI/RPP30 NRAS 46,XYt(8,21) (q22,q22)[2]/246,XX(2] 46,XY(8,21) (q22,q22)[2]/246,XX(2]	AML3	Unclassifiable	4	M	96	2.4	66	
AML6 MS 14 M 86 259 116 AML7 M4 12 M 98 20.5 17 AML8 M2 10 M 86 4.19 51 AML9 M5 10 F 97 2.2 191 AML10 M4 5 M 86 27.83 25 AML11 M4 7 M 107 92.92 36 AML12 M2 7 M 106 25.04 145 ID Gene fusion Gene mutation Cytogenetics AML1 PML/RARA FLT3-ITD 46,XY AML2 PML/RARA FLT3-ITD 46,XY 46,XY AML3 RUNX/RUNX1T1 NRAS, KIT, IDH 45,X,-Yt(8,21) (q22,q22)[11]/46,XY[5] AML4 NPM1/RP30 NRAS CREBBP, STATSA 46,XY2(5,10)(q34,q23)[14]/46,XX[6] AML5 MLL/AF6 FP3, ETV6 46,XY2(0] 46,XY2(0] AML6 <	AML4	Unclassifiable	1	M	102	26	50	
AML7 M4 12 M 98 20.5 17 AML8 M2 10 M 86 4.19 51 AML9 M5 10 F 97 2.2 191 AML10 M4 5 M 86 27.83 25 AML11 M4 7 M 107 92.92 36 AML12 M2 7 M 106 25.04 145 ID Gene fusion Gene mutation Cytogenetics AML1 PML/RARA FLT3-ITD 46,XY AML2 PML/RARA FLT3-ITD 46,XY,*(15,17),(q24,q21) AML3 RUNX/RUNX1T1 NRAS, KIT, IDH2 45,X-*,t(8,21) (q22,q22)[11]/46,XX[6] AML4 NPM1/RPP30 NRAS 46,XY,t(5,10)(q34,q23)[14]/46,XX[6] AML5 MLL/AF6 CREBBP, STAT5A 46,XY,t(5,10)(q34,q23)[13]/46,XX[2] AML6 MLL/AF9 TP53, ETV6 47,XY, + 8,t(9,11)(p22,q23)[20] AML7 NCOR2/UBC KRAS, ETT3-TKD, FLT3- ITD, KIT V,t(2;4) (q22;q21)[17]/46,XY[1] AML9 DEK/CAN <th< th=""><th>AML5</th><th>M5</th><th>2</th><th>F</th><th>96</th><th>123</th><th>274</th></th<>	AML5	M5	2	F	96	123	274	
AMIL8 M2 10 M 86 4.19 51 AML9 M5 10 F 97 2.2 191 AML10 M4 5 M 86 27.83 25 AML11 M4 7 M 107 92.92 36 AML12 M2 7 M 106 25.04 145 ID Gene fusion Gene mutation Cytogenetics AML1 PML/RARA FLT3-ITD 46,XY AML2 PML/RARA FLT3-ITD 46,XY,t(15,17),(q24,q21) AML3 RUNX/RUNXIT1 NRAS, KIT, IDH2 45,X-Y,t(8,21) (q22,q22)[11]/46,XY[5] AML4 NPM1/RPP30 NRAS 46,XY,t(5,10)(q34,q23)[14]/46,XX[6] AML5 MLL/AF6 CREBBP, STAT5A 46,XY,t(8,11)(q22,q23)[14]/46,XX[2] AML6 MLL/AF9 TP53, ETV6 46,XY,t(8,21)(q22,q22)[2] /45,idem,-Y,t(2,4) (q22,q21)[17]/46,XY[1] AML9 DEK/CAN KARS, U2AF1, EP300 46,XY AML10 ND CEBPA, CSF3R	AML6	M5	14	М	86	259	116	
AML9 M5 10 F 97 2.2 191 AML10 M4 5 M 86 27.83 25 AML11 M4 7 M 107 92.92 36 AML12 M2 7 M 106 25.04 145 ID Gene fusion Gene mutation Cytogenetics AML1 PML/RARA FLT3-ITD 46,XY AML2 PML/RARA FLT3-ITD 46,XY 146,XY/15,17),(q24,q21) AML3 RUNX/RUNXIT1 NRAS, KIT, IDH2 45,X,-Y,t(8,21) (q22,q22)[11]/46,XY[6] AML4 NPM1/RPP30 NRAS 46,XY,t(5,10)(q34,q23)[14]/46,XX[6] AML5 AML4 MLL/AF6 CREBBP, STAT5A 46,XX,del(11)(q22)[13]/46,XX[2] AML5 AML6 MLL/AF9 TP53, ETV6 47,XY, + 8,t(9,11)(p22,q23)[20] AML7 AML7 NCOR2/UBC KRAS, ET3-TKD, FLT3- ITD, KIT FLT3- ITD, KIT 46,XY(16,21)(q22;q22)[2] /45,idem,- Y,t(2;4) (q22;q22)[2] /45,idem,- Y,t(2;4) (q22;q22)[2] /45,idem,- Y,t(2;4) (q22;q22)[17]/46,XY[1] AML9 DEK/CAN KARS, U2AF1, EP300 46,XY <	AML7	M4	12	M	98	20.5	17	
AML10 M4 5 M 86 27.83 25 AML11 M4 7 M 107 92.92 36 AML12 M2 7 M 106 25.04 145 ID Gene fusion Gene mutation Cytogenetics AML1 PML/RARA FLT3-ITD 46,XY AML2 PML/RARA FLT3-ITD 46,XY,t(15,17),(q24,q21) AML3 RUNX/RUNX1T1 NRAS, KIT, IDH2 45,X,-Y,t(8,21) (q22,q22)[11]/46,XY[5] AML4 NPM1/RPP30 NRAS 46,XY,t(5,10)(q34,q23)[14]/46,XY[6] AML5 MLL/AF6 CREBBP, STAT5A 46,XX,del(11)(q22)[13]/46,XX[2] AML6 MLL/AF9 TP53, ETV6 47,XY, + 8,t(9,11)(p22,q23)[20] AML7 NCOR2/UBC KRAS, ETV6 46,XY(20] AML8 RUNX/RUNX1T1 NRAS, FLT3-TKD, FLT3- ITD, KIT HX,12,4) (q22;q22)[2] /45,idem,- Y,t(2;4) (q22;q21)[17]/46,XY[1] AML9 DEK/CAN KARS, U2AF1, EP300 46,XY AML10 ND CEBPA, CSF3R 46,XY	AML8	M2	10	М	86	4.19	51	
AML11 M4 7 M 107 92.92 36 AML12 M2 7 M 106 25.04 145 ID Gene fusion Gene mutation Cytogenetics AML1 PML/RARA FLT3-ITD 46,XY,t(15,17),(q24,q21) AML2 PML/RARA FLT3-ITD 46,XY,t(15,17),(q24,q21) AML3 RUNX/RUNX1T1 NRAS, KIT, IDH2 45,X,-Y,t(8,21) (q22,q22)[11]/46,XY[5] AML4 NPM1/RPP30 NRAS 46,XY,t(5,10)(q34,q23)[14]/46,XY[6] AML5 MLL/AF6 CREBBP, STAT5A 46,XX,del(11)(q22)[13]/46,XX[2] AML6 MLL/AF9 TP53, ETV6 47,XY, + 8,t(9,11)(p22,q23)[20] AML7 NCOR2/UBC KRAS, ETV6 46,XY;(8;21)(q22;q22)[2] /45,idem, 1TD, KIT AML8 RUNX/RUNX1T1 NRAS, FLT3-TKD, FLT3- 1TD, FLT3- 1TD, KIT 46,XY;(8;21)(q22;q22)[2] /45,idem, Y;(2;4) (q22;q21)[17]/46,XY[1] AML9 DEK/CAN KARS, U2AF1, EP300 46,XY AML10 ND CEBPA, CSF3R 46,XY AML11 MLL/AF9 NF1 46,XY,(9,11)(p21,q22)	AML9	M5	10	F	97	2.2	191	
AML12 M2 7 M 106 25.04 145 ID Gene fusion Gene mutation Cytogenetics AML1 PML/RARA FLT3-ITD 46,XY AML2 PML/RARA FLT3-ITD 46,XY,t(15,17),(q24,q21) AML3 RUNX/RUNX1T1 NRAS, KIT, IDH2 45,X,-Y,t(8,21) (q22,q22)[11]/46,XY[5] AML4 NPM1/RPP30 NRAS 46,XY,t(5,10)(q34,q23)[14]/46,XY[6] AML5 MLL/AF6 CREBBP, STAT5A 46,XY,del(11)(q22)[13]/46,XX[2] AML6 MLL/AF9 TP53, ETV6 47,XY, + 8,t(9,11)(p22,q23)[20] AML7 NCOR2/UBC KRAS, ETV6 46,XY[20] AML8 RUNX/RUNX1T1 NRAS, FLT3-TKD, FLT3- ITD, KIT FLT3- ITD, KIT Y,t(2;4) (q22;q22)[2] /45,idem,- Y,t(2;4) (q22;q22)[17]/46,XY[1] AML9 DEK/CAN KARS, U2AF1, EP300 46,XY AML10 ND CEBPA, CSF3R 46,XY AML11 MLL/AF9 NF1 46,XY;t(9,11)(p21,q22)[14]/46,XY	AML10	M4	5	M	86	27.83	25	
ID Gene fusion Gene mutation Cytogenetics AML1 PML/RARA FLT3-ITD 46,XY AML2 PML/RARA FLT3-ITD 46,XY,t(15,17),(q24,q21) AML3 RUNX/RUNX1T1 NRAS, KIT, IDH2 45,X-Y,t(8,21) (q22,q22)[11]/46,XY[5] AML4 NPM1/RPP30 NRAS 46,XY,t(5,10)(q34,q23)[14]/46,XY[6] AML5 MLL/AF6 CREBBP, STAT5A 46,XX,del(11)(q22)[13]/46,XX[2] AML6 MLL/AF9 TP53, ETV6 47,XY, + 8,t(9,11)(p22,q23)[20] AML7 NCOR2/UBC KRAS, ETV6 46,XY[20] AML8 RUNX/RUNX1T1 NRAS, FLT3-TKD, FLT3- ITD, KIT 46,XY;t(8;21)(q22;q22)[2] /45,idem,- Y,t(2;4) (q22;q21)[17]/46,XY[1] AML9 DEK/CAN KARS, U2AF1, EP300 46,XY AML10 ND CEBPA, CSF3R 46,XY AML11 MLL/AF9 NF1 46,XY;t(9,11)(p21,q22)[14]/46,XY	AML11	M4	7	M	107	92.92	36	
AML1 PML/RARA FLT3-ITD 46,XY AML2 PML/RARA FLT3-ITD 46,XY,t(15,17),(q24,q21) AML3 RUNX/RUNX1T1 NRAS, KIT, IDH2 45,X,-Y,t(8,21) (q22,q22)[11]/46,XY[5] AML4 NPM1/RPP30 NRAS 46,XY,t(5,10)(q34,q23)[14]/46,XX[6] AML5 MLL/AF6 CREBBP, STAT5A 46,XX,del(11)(q22)[13]/46,XX[2] AML6 MLL/AF9 TP53, ETV6 47,XY, + 8,t(9,11)(p22,q23)[20] AML7 NCOR2/UBC KRAS, ETV6 46,XY[20] AML8 RUNX/RUNX1T1 NRAS, FLT3-TKD, FLT3- ITD, KIT 46,XY,t(8;21)(q22;q22)[2] /45,idem,- Y,t(2;4) (q22;q21)[17]/46,XY[1] AML9 DEK/CAN KARS, U2AF1, EP300 46,XY AML10 ND CEBPA, CSF3R 46,XY AML11 MLL/AF9 NF1 46,XY,t(9,11)(p21,q22)[14]/46,XY	AML12	M2	7	M	106	25.04	145	
AML2 PML/RARA FLT3-ITD 46,XY;t(15,17),(q24,q21) AML3 RUNX/RUNX1T1 NRAS, KIT, IDH2 45,X,-Y;t(8,21) (q22,q22)[11]/46,XY[5] AML4 NPM1/RPP30 NRAS 46,XY;t(5,10)(q34,q23)[14]/46,XX[6] AML5 MLL/AF6 CREBBP, STAT5A 46,XX,del(11)(q22)[13]/46,XX[2] AML6 MLL/AF9 TP53, ETV6 47,XY, + 8,t(9,11)(p22,q23)[20] AML7 NCOR2/UBC KRAS, ETV6 46,XY[20] AML8 RUNX/RUNX1T1 NRAS, FLT3-TKD, FLT3- ITD, KIT 46,XY;t(8;21)(q22;q22)[2] /45,idem,- Y;t(2;4) (q22;q21)[17]/46,XY[1] AML9 DEK/CAN KARS, U2AF1, EP300 46,XY AML10 ND CEBPA, CSF3R 46,XY AML11 MLL/AF9 NF1 46,XY;t(9,11)(p21,q22)[14]/46,XY	ID	Gene fusion		Gene mu	tation	Cytogenetics	Cytogenetics	
AML3 RUNX/RUNX1T1 NRAS, KIT, IDH2 45,X,-Y,t(8,21) (q22,q22)[11]/46,XY[5] AML4 NPM1/RPP30 NRAS 46,XY,t(5,10)(q34,q23)[14]/46,XX[6] AML5 MLL/AF6 CREBBP, STAT5A 46,XX,del(11)(q22)[13]/46,XX[2] AML6 MLL/AF9 TP53, ETV6 47,XY, + 8,t(9,11)(p22,q23)[20] AML7 NCOR2/UBC KRAS, ETV6 46,XY[20] AML8 RUNX/RUNX1T1 NRAS, FLT3-TKD, FLT3- ITD, KIT 46,XY,t(8;21)(q22;q22)[2] /45,idem,- Y,t(2;4) (q22;q21)[17]/46,XY[1] AML9 DEK/CAN KARS, U2AF1, EP300 46,XY AML10 ND CEBPA, CSF3R 46,XY AML11 MLL/AF9 NF1 46,XY,t(9,11)(p21,q22)[14]/46,XY	AML1	PML/RARA		FLT3-ITD		46,XY	46,XY	
AML4 NPM1/RPP30 NRAS 46,XY,t(5,10)(q34,q23)[14]/46,XX[6] AML5 MLL/AF6 CREBBP, STAT5A 46,XX,del(11)(q22)[13]/46,XX[2] AML6 MLL/AF9 TP53, ETV6 47,XY, + 8,t(9,11)(p22,q23)[20] AML7 NCOR2/UBC KRAS, ETV6 46,XY[20] AML8 RUNX/RUNX1T1 NRAS, FLT3-TKD, FLT3- ITD, KIT 46,XY,t(8;21)(q22;q22)[2] /45,idem,- Y,t(2;4) (q22;q21)[17]/46,XY[1] AML9 DEK/CAN KARS, U2AF1, EP300 46,XY AML10 ND CEBPA, CSF3R 46,XY AML11 MLL/AF9 NF1 46,XY,t(9,11)(p21,q22)[14]/46,XY	AML2	PML/RARA		FLT3-ITD		46,XY,t(15,17),(q24,c	46,XY,t(15,17),(q24,q21)	
AML5 MLL/AF6 CREBBP, STAT5A 46,XX,del(11)(q22)[13]/46,XX[2] AML6 MLL/AF9 TP53, ETV6 47,XY, + 8,t(9,11)(p22,q23)[20] AML7 NCOR2/UBC KRAS, ETV6 46,XY[20] AML8 RUNX/RUNX1T1 NRAS, FLT3-TKD, FLT3- ITD, KIT 46,XY,t(8;21)(q22;q22)[2] /45,idem,- Y,t(2;4) (q22;q21)[17]/46,XY[1] AML9 DEK/CAN KARS, U2AF1, EP300 46,XY AML10 ND CEBPA, CSF3R 46,XY AML11 MLL/AF9 NF1 46,XY,t(9,11)(p21,q22)[14]/46,XY	AML3	RUNX/RUNX1T1		NRAS, KIT	, IDH2	45,X,-Y,t(8,21) (q22,d	45,X,-Y,t(8,21) (q22,q22)[11]/46,XY[5]	
AML6 MLL/AF9 TP53, ETV6 47,XY, + 8,t(9,11)(p22,q23)[20] AML7 NCOR2/UBC KRAS, ETV6 46,XY[20] AML8 RUNX/RUNX1T1 NRAS, FLT3-TKD, FLT3- ITD, KIT 46,XY,t(8;21)(q22;q22)[2] /45,idem,- Y,t(2;4) (q22;q21)[17]/46,XY[1] AML9 DEK/CAN KARS, U2AF1, EP300 46,XY AML10 ND CEBPA, CSF3R 46,XY AML11 MLL/AF9 NF1 46,XY,t(9,11)(p21,q22)[14]/46,XY	AML4	NPM1/RPP30		NRAS		46,XY,t(5,10)(q34,q2	46,XY,t(5,10)(q34,q23)[14]/46,XX[6]	
AML7 NCOR2/UBC KRAS, ETV6 46,XY[20] AML8 RUNX/RUNX1T1 NRAS, FLT3-TKD, FLT3- ITD, KIT 46,XY,t(8;21)(q22;q22)[2] /45,idem,- Y,t(2;4) (q22;q21)[17]/46,XY[1] AML9 DEK/CAN KARS, U2AF1, EP300 46,XY AML10 ND CEBPA, CSF3R 46,XY AML11 MLL/AF9 NF1 46,XY,t(9,11)(p21,q22)[14]/46,XY	AML5	MLL/AF6		CREBBP, S	TAT5A	46,XX,del(11)(q22)[1	46,XX,del(11)(q22)[13]/46,XX[2]	
AML8 RUNX/RUNX1T1 NRAS, FLT3-TKD, FLT3- ITD, KIT 46,XY,t(8;21)(q22;q22)[2] /45,idem,- Y,t(2;4) (q22;q21)[17]/46,XY[1] AML9 DEK/CAN KARS, U2AF1, EP300 46,XY AML10 ND CEBPA, CSF3R 46,XY AML11 MLL/AF9 NF1 46,XY,t(9,11)(p21,q22)[14]/46,XY	AML6	MLL/AF9		TP53, ETV	6	47,XY, +8,t(9,11)(p2	47,XY, + 8,t(9,11)(p22,q23)[20]	
AML9 DEK/CAN KARS, U2AF1, EP300 46,XY AML10 ND CEBPA, CSF3R 46,XY AML11 MLL/AF9 NF1 46,XY,t(9,11)(p21,q22)[14]/46,XY	AML7	NCOR2/UBC		KRAS, ET\	/6	46,XY[20]	46,XY[20]	
AML10 ND CEBPA, CSF3R 46,XY AML11 MLL/AF9 NF1 46,XY,t(9,11)(p21,q22)[14]/46,XY	AML8	RUNX/RUNX1T1			3-TKD, FLT3-		· · · · · · · · · · · · · · · · · · ·	
AML11 MLL/AF9 NF1 46,XY,t(9,11)(p21,q22)[14]/46,XY	AML9	DEK/CAN		KARS, U2	AF1, EP300	46,XY	46,XY	
	AML10	ND		CEBPA, CS	SF3R	46,XY	46,XY	
AML12 RUNX/RUNX1T1 KIT, ASXL2, DHX15 45,X,-Y,t(8,21) (q22,q22)[4]/46,XY[12]	AML11	MLL/AF9		NF1		46,XY,t(9,11)(p21,q2	46,XY,t(9,11)(p21,q22)[14]/46,XY	
	AML12	RUNX/RUNX1T1		KIT, ASXL	2, DHX15	45,X,-Y,t(8,21) (q22,0	45,X,-Y,t(8,21) (q22,q22)[4]/46,XY[12]	

The heatmaps associated with these pathways were shown below (Fig. 4C–F). In accordance with the aforementioned phenotypic analyses, ANA treatment precipitated a time-dependent reduction in the levels of phosphorylated ERK1/2, p38, JNK, and ERK5, as observed at the protein level using western blotting (Fig. 4G), Additionally, the heatmaps highlighted a notable transcriptional downregulation of Cyclin D1 (Fig. 4C, D). To verify these results, we performed RNA sequencing analysis of primary cells from AML patient #6, which yielded convincing results. GSEA of RNA sequencing data from AML patient #6 showed that cell cycle-related genes were significantly enriched. The heatmap showed that ERK1/2 cascade-related genes were significantly downregulated (Supplementary Fig. 2A, B).

In summary, ANA suppressed the growth of high PDE3A-expressing AML cells through the downregulation of the MAPK signaling pathway in high PDE3A-expressing AML cells.

Notable synergistic effect of anagrelide combined with idarubicin in high PDE3A-expressing AML cells

Notably, the heatmaps depicting the altered gene expression within the four aforementioned signaling pathways demonstrated that genes associated with drug resistance mechanisms, including PAK1, p-SRC, DUSP16, and EGR1, exhibited distinct downregulation at the transcriptional level (Fig. 4 C–E). RNA sequencing analysis also showed PAK1 and EGR1 were down-regulated in primary cells from AML patient #6 (Supplementary Fig. 2C). Recent studies have reported that these genes contribute to drug resistance and highlighted the potential of targeting these genes to overcome drug resistance in cancers [26–30]. Western blotting revealed that ANA treatment rapidly decreased p-SRC, PAK1, EGR1, and DUSP16 protein levels in a time-dependent manner

(Fig. 4H). This treatment may enhance the sensitivity of AML cells to drugs most often used in the treatment of pediatric AML patients.

To evaluate the effect of ANA on the sensitivity of high PDE3Aexpressing AML cells to chemotherapeutic drugs and select effective drugs combined with ANA, we determined the concentrations of idarubicin (IDA), homoharringtonine (HHT), daunorubicin (DNR), cytarabine (Ara-C), etoposide (VP-16), decitabine (DEC), and cladribine (Clad) that only caused minimal cell suppression within 72 h; then, ANA was combined with individual anti-leukemia drugs in a concentration-dependent manner to investigate their synergistic and sequential effects on inhibiting the proliferation of HEL and MOLM-16 cells. Simultaneous treatment with IDA and ANA for 72 h significantly reduced the growth rate of HEL and MOLM-16 cells (Fig. 5A, B), and the combination index at various doses was approximately <1 (Fig. 5C, D). Simultaneous treatment with HHT and ANA reduced the growth rate of HEL and MOLM-16 cells. However, the effect of HHT combined with ANA was inferior to that of IDA combined with ANA (Fig. 5E-H). IDA combined with ANA had the strongest synergistic effect among the seven anti-leukemia drugs, depending on the IC₅₀ for cell proliferation at an ineffective concentration of chemotherapeutic agents (Supplementary Fig. 3A-E). To verify the effect of combined medication in high PDE3A-expressing AML cells, primary cells from AML patients in the PDE3A high group (n = 6) determined based on the median PDE3A expression at the transcriptional level were treated with vehicle control, 0.005 µM IDA, 5 μM ANA, and 0.005 μM IDA with 5 μM ANA. Consistent with the results of the cell line experiment, the combination treatment with IDA and ANA significantly reduced cell viability compared with the use of a single agent. Notably, the combination of ANA

 Table 2.
 Baseline characteristics of patients in the PDE3A-high and PDE3A-low cohorts.

Characteristic	All patients (N = 148)	PDE3A Low (<i>N</i> = 37)	PDE3AHigh (<i>N</i> = 111)	<i>P</i> -value
Age, years (%)				0.2412
<1	6 (4.1)	1 (2.7)	5 (4.5)	
≥1, <10	95 (64.2)	28 (75.7)	67 (60.4)	
≥10	47 (31.8)	8 (21.6)	39 (35.1)	
Sex (%)				0.5638
Male	86 (58.1)	23 (62.2)	63 (56.8)	
Female	62 (41.9)	14 (37.8)	48 (43.2)	
Leukocyte count at diagnosis, x10 ⁹ /L (%)				0.6361
≥100	29 (19.6)	9 (24.3)	20 (18.0)	
≥50, <100	26 (17.6)	7 (18.9)	19 (17.1)	
<50	93 (62.8)	21 (56.8)	72 (64.9)	
Hemoglobin (median, range, g/L)	79 (25–129)	77 (33–120)	80 (25–129)	0.7267
Platelet (median, range, ×10 ⁹ /L)	55 (5–396)	58 (6–217)	55 (5–396)	0.8939
FAB				0.4431
M1	1 (0.7)	0 (0.0)	1 (0.9)	
M2	69 (46.6)	13 (35.1)	56 (50.5)	
M3	2 (1.4)	0 (0.0)	2 (1.8)	
M4	21 (14.2)	10 (27.0)	21 (18.9)	
M5	35 (23.6)	11 (29.7)	24 (21.6)	
M7	6 (4.1)	0 (0.0)	6 (5.4)	
Unclassified	16 (10.8)	3 (8.1)	13 (11.7)	
Karyotype (%)		· (
Normal	36 (24.3)	4 (10.8)	32 (28.8)	0.02
Chromosome 5, 7 abnormalities	2 (1.4)	0 (0.0)	2 (1.8)	1
Complex	7 (4.7)	1 (2.7)	6 (5.4)	0.6774
Not evaluable	8 (5.4)	1 (2.7)	7 (6.3)	0.6798
Fusions (%)			· ·	
RUNX1::RUNX1T1	52 (35.1)	10 (27.0)	42 (37.8)	0.2329
CBFB::MYH11	19 (12.8)	10 (27.0)	9 (8.1)	0.008
KMT2A::MLLT3	7 (4.7)	3 (8.1)	4 (3.6)	0.367
KMT2A:: MLLT11	1 (0.7)	1 (2.7)	0 (0.0)	0.25
Other KMT2A rearrangements	11 (7.4)	8 (21.6)	3 (2.7)	0.0007
NUP98 rearrangements	9 (6.1)	1 (2.7)	8 (7.2)	0.4511
Other high-risk fusions †	7 (4.7)	0 (0.0)	7 (6.3)	0.1929
Other unknown fusions	11 (7.4)	2 (5.4)	9 (8.1)	0.7315
Mutations (%)	11 (7.4)	2 (5.4)	5 (0.1)	0.7515
CEBPA double mutations	14 (9.5)	1 (2.7)	13 (11.7)	0.1905
NPM1	9 (6.1)	1 (2.7)	8 (7.2)	0.4511
KIT	37 (25.0)	9 (24.3)		0.4311
FLT3-ITD	15 (10.1)	2 (5.4)	28 (25.2) 13 (11.7)	0.3582
Other high-risk mutations*	12 (8.1)	4 (10.8)	8 (7.2)	0.4955
Induction regimen	75 (50.7)	15 (40 5)	60 (F4.1)	0.1854
LDC	75 (50.7)	15 (40.5)	60 (54.1)	
SDC	73 (49.3)	22 (59.5)	51 (45.9)	0.773.
HSCT with CR1	05 (57.4)	22 (50 5)	(2 (5(0)	0.7734
Yes	85 (57.4)	22 (59.5)	63 (56.8)	
No	63 (42.6)	15 (40.5)	48 (43.2)	

The bold values mean that the P value is <0.05, and the results have statistical significance. 0.02 showed that in normal karyotype, the patients with high expression of PDE3A were more than the patients with low expression of PDE3A. 0.008 and 0.0007 showed that PDE3A exhibits low expression levels in specific fusions of AML, including CBFB-MYH11 and other KMT2A rearrangements (except KMT2A-MLLT3 and KMT2A-MLLT11).

Other high-risk fusions included DEK::NUP214, BCR::ABL1, ETV6::MNX1, TLS::ERG and CBFA2T3::GLIS2.

CNS central nervous system, CEBPA CCAAT enhancer-binding protein alpha, NPM1 nucleophosmin 1, KIT KIT proto-oncogene receptor tyrosine kinase, FLT3-ITD FMS-like tyrosine kinase 3 gene internal tandem duplication, RUNX1 RUNX family transcription factor 1, ASXL1 ASXL transcriptional regulator 1, TP53 tumor protein p53, HSCT hematopoietic stem cell transplantation.

^{*}Other high-risk mutations include RUNX1, ASXL1, and TP53.

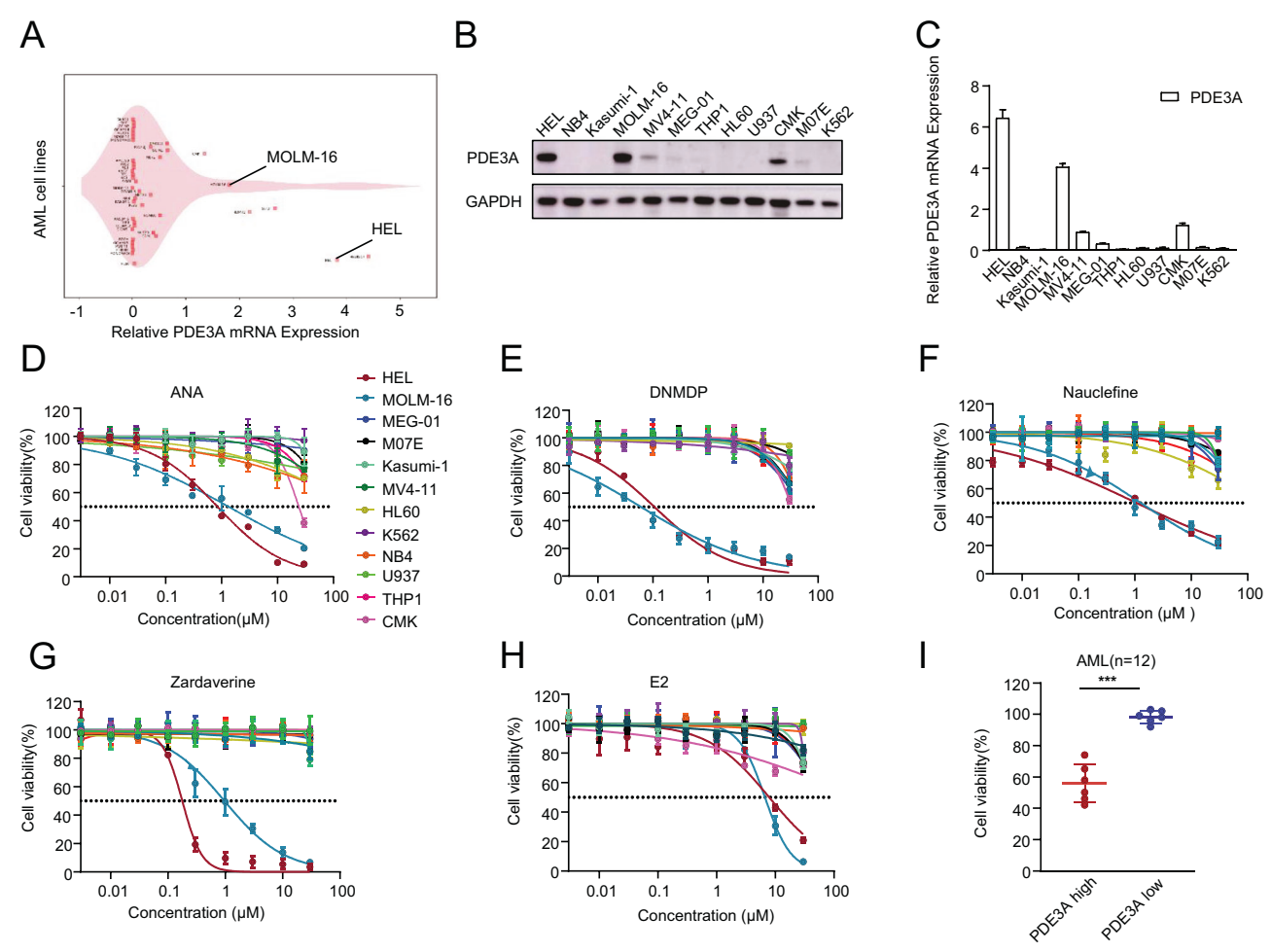


Fig. 2 PDE3A inhibitors specifically inhibiting the growth of high PDE3A-expressing AML cells. A Violin plot of PDE3A expression in the CCLE data set of AML cells. **B** Western blot analysis of PDE3A protein levels in AML cells and normalized to that of GAPDH. **C** Relative mRNA expression of PDE3A in AML cells quantified using qRT-PCR and normalized to that of GAPDH. A CCK-8 assay of cell viability in the leukemic cells treated with the corresponding concentrations of PDE3A inhibitors ANA **D**, DNMDP **E**, nauclefine **F**, zardaverine **G**, and E2 **H** for 72 h. The IC₅₀ values were calculated based on the drug concentrations that cause 50% cell viability. **I** Primary BMMNCs from patients with AML (n = 12) were divided into two groups: PDE3A^{high} group (n = 6) and PDE3A^{low} group (n = 6). The cell viability were determined via the CCK-8 assay following treatment with 5 μM ANA for 72 h. Data are presented as the mean ± SD (n = 3). Comparisons were evaluated using the two-tailed Student's *t*-test, and multiple groups were analyzed using a one-way analysis of variance. *P < 0.05, **P < 0.01, ****P < 0.001, *****P < 0.0001, NS not significant.

and IDA showed minimal impact to primary cells from AML patients in the PDE3A low group (n = 6) (Fig. 5I).

To explore the effect of each treatment on the proliferative ability and self-renewal ability of the primary PDE3A^{high} AML sample, we treated the primary cells from AML patient #6 with PBS (control), 5 μM ANA, 0.005 μM IDA and 5 μM ANA combined with 0.005 μM IDA. Consistently, ANA combined with IDA inhibited the colony-forming ability of the primary cells obtained from the PDE3A^{high} AML patient to a greater extent compared with single-drug treatment (Fig. 5J). Serial colony-forming assay indicated that IDA combined with ANA significantly inhibited the self-renewal ability of primary PDE3A^{high} AML sample (Fig. 5K).

Together, ANA combined with IDA had a synergistic effect on both AML cell lines and primary cells from AML patients with high PDE3A expression.

ANA combined with IDA synergistically inhibiting the growth of high PDE3A-expressing AML cell lines through pyroptosis by triggering GSDME cleavage

To unravel the intricate molecular mechanisms underlying the synergistic antileukemic effects of ANA in combination with IDA, RNA sequencing analysis of HEL cells was conducted. Our

comprehensive data analysis revealed that treatment with a combination of ANA and IDA within 72 h engendered significant transcriptional modifications. This combined treatment led to the upregulation of 906 genes and substantial downregulation of 777 genes (adjusted P-value < 0.05 and an absolute log₂ fold-change > 0.5) (Fig. 6A). KEGG analysis showed that categories related to "neutrophil extracellular trap formation," "MAPK signaling path-"alcoholism," and "systemic lupus erythematosus" highly enriched (Fig. 6B). Notably, a recent study has indicated that the inhibition of the MAPK signaling pathway can mitigate inflammation, a phenomenon corroborated by the findings presented in Fig. 4E [31–33]. The pro-inflammatory factor IL-1\u00bb exhibited an upregulated expression upon treatment with ANA combined with IDA (Fig. 6C). To validate the observations from the heatmap analysis, a comprehensive functional annotation and enrichment analysis of the DEGs was performed, utilizing the HALLMARK pathway enrichment approach. Combination treatment with IDA and ANA led to positive enrichment of the inflammatory response pathway (Fig. 6D) and the KRAS signaling pathway (upstream of the MAPK signaling pathway) (Fig. 6E).

Given the notably elevated expression of inflammatory factors in AML cells, the mode of cell death possibly involved pyroptosis,

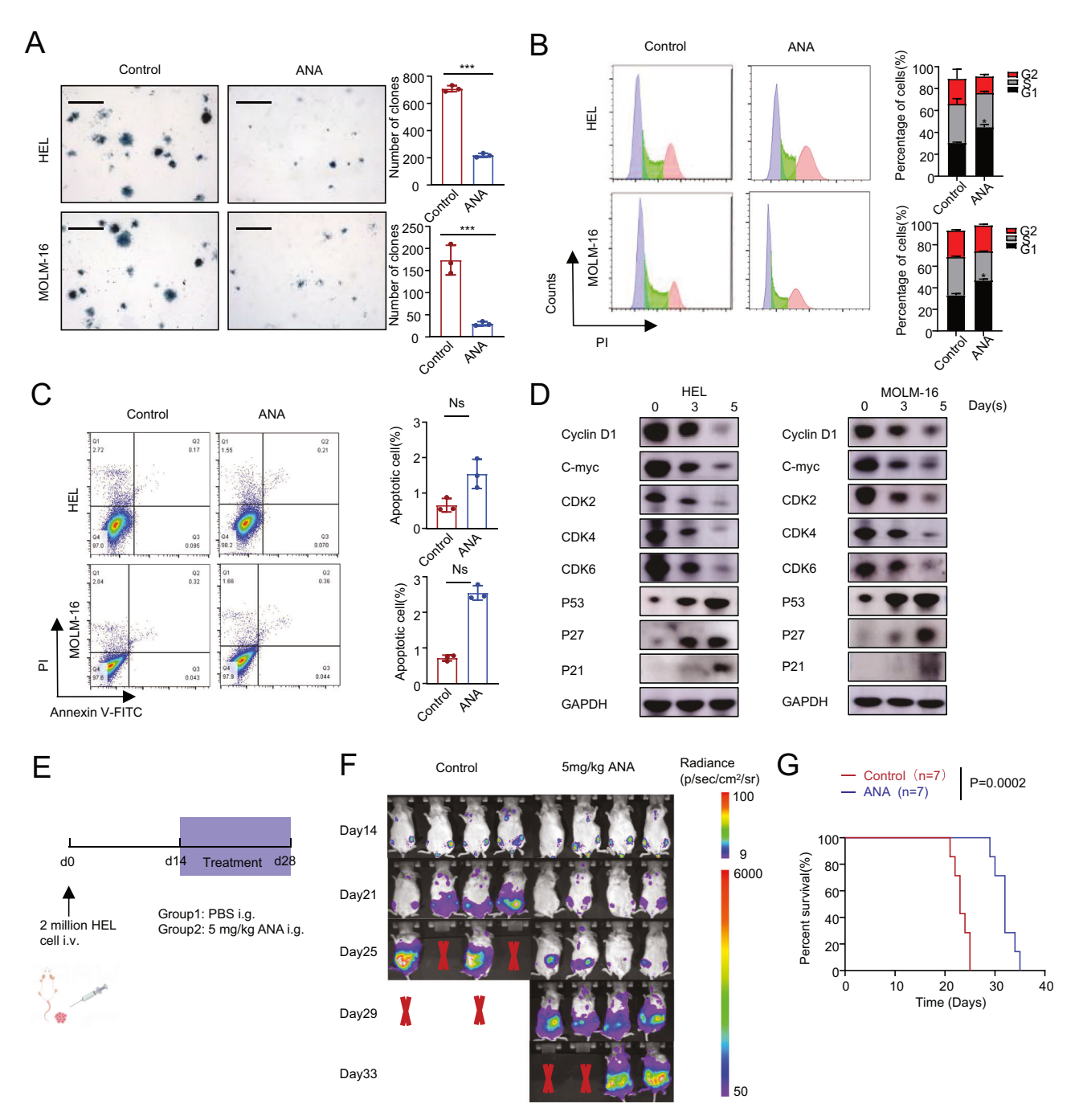
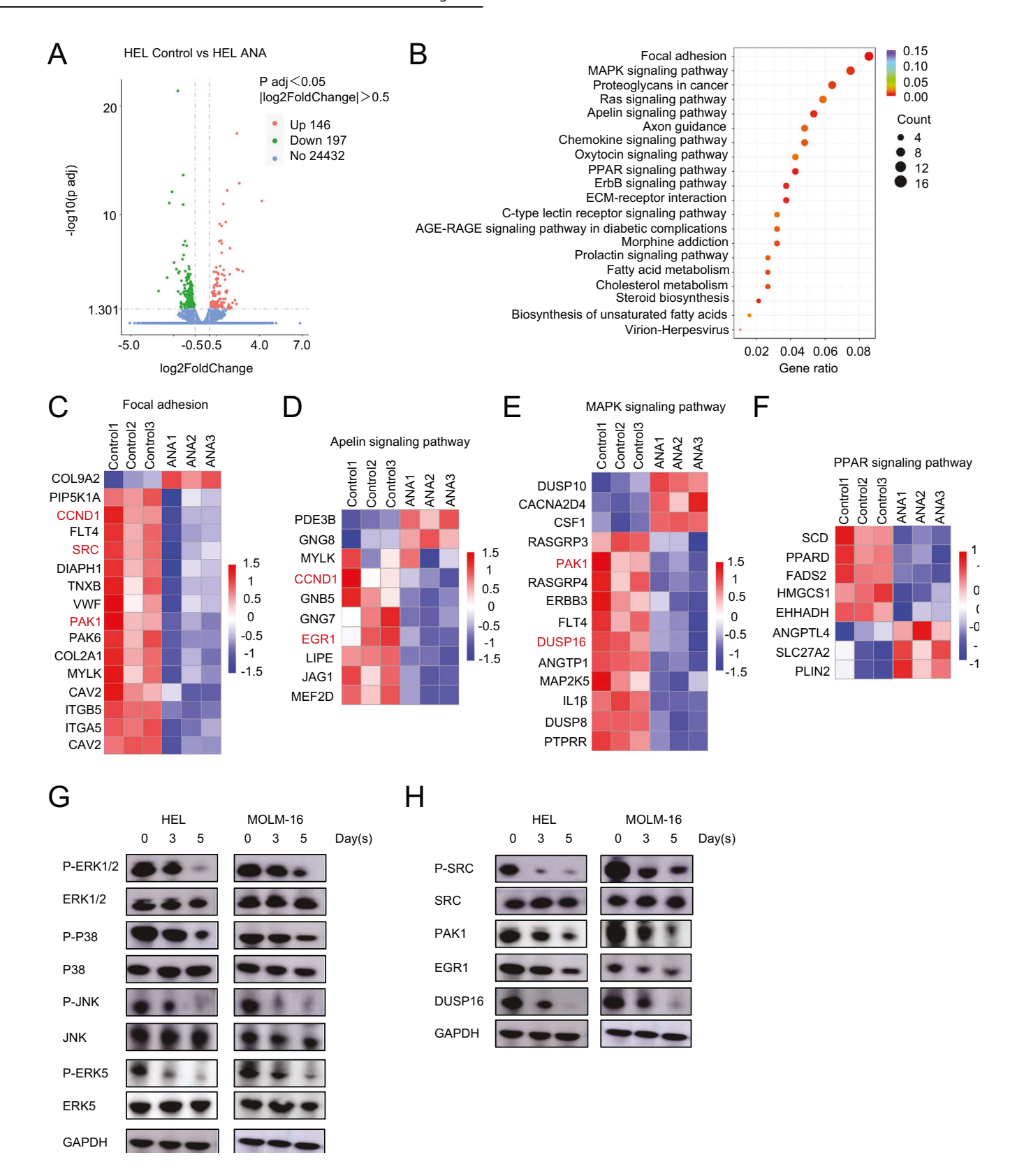


Fig. 3 ANA suppressing the proliferation of high PDE3A-expressing AML cell lines by interrupting the cell cycle and inhibiting colony-forming capacity. A Colony formation in HEL and MOLM-16 cells as determined by cell counting and the colony-forming assay (scale bar: 200 μ m). B Cell cycle distribution of HEL and MOLM-16 cells as determined via flow cytometric analysis of PI staining. C Cell apoptosis of HEL and MOLM-16 cells as determined using flow cytometric analysis of Annexin V-FITC, PI staining. D HEL and MOLM-16 cells were treated with 1 μ M ANA for 72 and 120 h and then subjected to western blot analysis to detect the changes in cell cycle-related proteins. E HEL cells were transfected with luciferase overexpressed and engrafted into the NSG mice (2 × 10⁶ cells per mouse); 14 days later, the mice were treated daily with vehicle treatment and 5 mg/kg ANA by gavage for 14 days (days 14–28). F Bioluminescence imaging of mice from each group (n=7) was obtained on days 14, 21, 25, 29, and 33. G The Kaplan–Meier survival curves of two cohorts of transplanted mice are shown. The P-values were determined using the log-rank test (n=7). Data are presented as the mean \pm SD (n=3). Comparisons were evaluated using the two-tailed Student's t-test, and multiple groups were analyzed using a one-way analysis of variance. *P < 0.05, **P < 0.01, ***P < 0.001, ****P < 0.0001, NS not significant.

necroptosis, and PANoptosis [34–37]. The RNA sequencing analysis showed that the genes associated with necroptosis only exhibited minimal changes at the mRNA level, while those related to pyroptosis such as GSDME and NLRP3 showed significant changes. Inflammatory factor IL-1 β was highly upregulated at the

mRNA levels (Fig. 6F). In the present study, consistent with the findings of previous RNA sequencing analyses, the expression levels of proteins associated with GSDME-mediated pyroptosis, including cleaved-CASP3, cleaved-CASP8, and cleaved GSDME-N were significantly upregulated when cells were treated with IDA



and ANA compared with the expression levels of those treated with IDA or ANA alone (Fig. 6G). ELISA of IL-1 β and IL-18 levels in the supernatant from cell cultures demonstrated that the secretion of IL-1 β and IL-18 was significantly upregulated when combination treatment with IDA and ANA was used compared

with IDA or ANA alone (Fig. 6H). To verify these results, we performed RNA sequencing analysis of primary cells from AML patient #6; concurrently, combination treatment with IDA and ANA positively enriched the inflammatory bowel disease and inflammatory mediator regulation of trp channels. The RNA

Fig. 4 Targeting PDE3A to downregulate the MAPK signaling pathway in high PDE3A-expressing AML cells. A Volcano plots of normalized gene expression in HEL cells with or without ANA treatment for 72 h as analyzed via RNA sequencing. B Kyoto Encyclopedia of Gene and Genomes (KEGG) analysis of these significant gene signatures from the corresponding normalized enrichment score (NES). Heatmap of differentially expressed genes in HEL cells treated with 1 μ M ANA in "focal adhesion" C, "apelin signaling pathway" D, "MAPK signaling pathway" E, and "PPAR signaling pathway" F. Each column represents a sample, each row represents a gene, blue represents the downregulation of genes, and red represents the upregulation of genes. G, H HEL and MOLM-16 cells were treated with 1 μ M ANA for 72 and 120 h, respectively, and then subjected to western blot analysis to detect any changes in the expression of related proteins. Data are presented as the mean \pm SD (n=3). Comparisons were evaluated using the two-tailed Student's t-test, and multiple groups were analyzed using a one-way analysis of variance. *t0.05, *t10, *t20.01, ****t20.001. NS not significant.

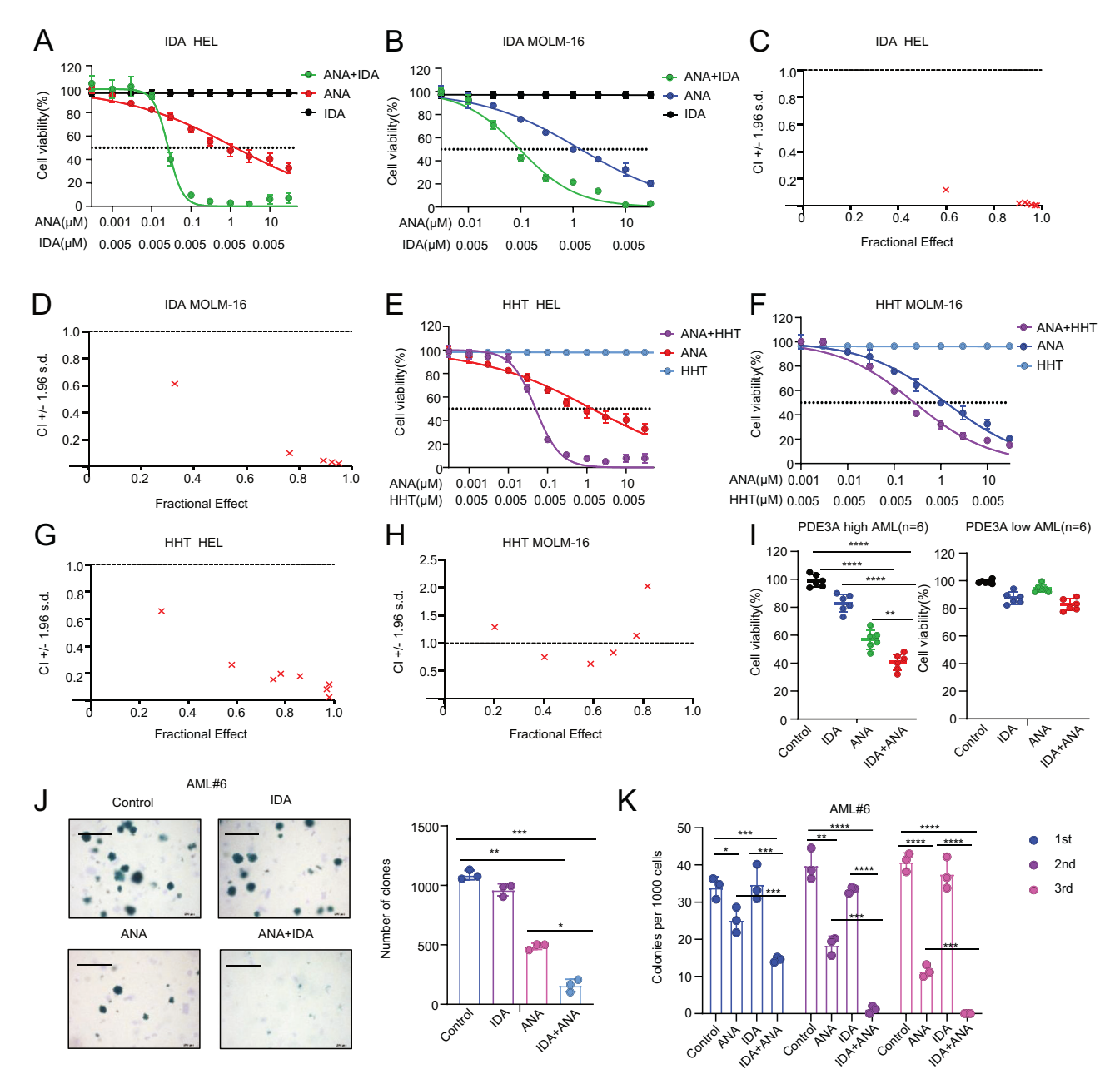
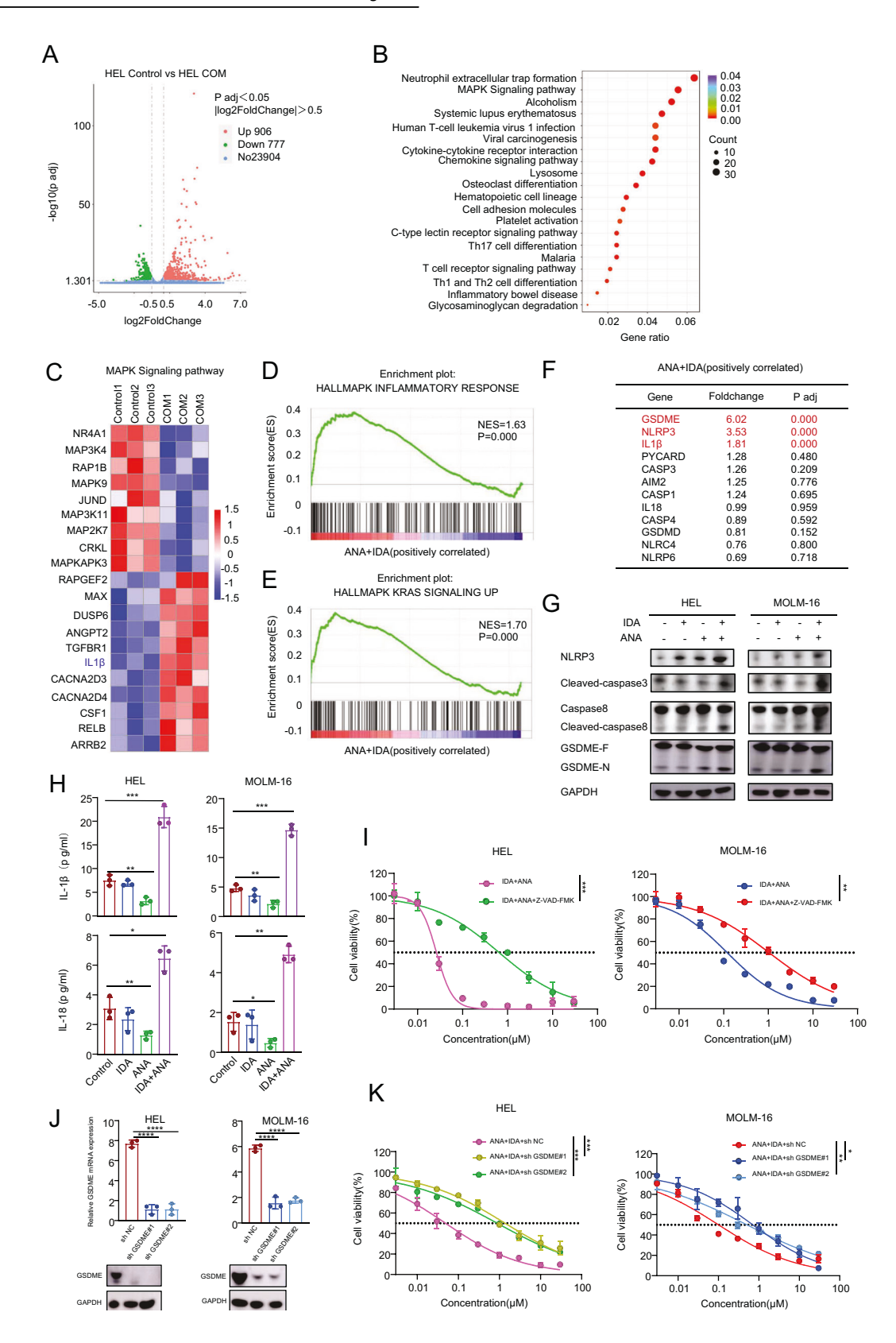


Fig. 5 ANA combined with IDA showing a notable synergistic effect in AML cells. A, B HEL and MOLM-16 were treated with the indicated concentrations of ANA and IDA for 72 h and then subjected to the CCK-8 assay to detect the anti-proliferative effect. C, D CI plots of ANA/IDA combinatorial treatment in HEL and MOLM-16 cells. E, F HEL and MOLM-16 were treated with the indicated concentrations of ANA and HHT for 72 h and then subjected to the CCK-8 assay to detect the anti-proliferative effect. G-H CI plots of ANA/HHT combinatorial treatment in HEL and MOLM-16 cells. I Primary BMMNCs from patients with AML in the PDE3A^{high} group (n = 6) and PDE3A^{low} group (n = 6) were determined via the CCK-8 assay following the treatment of DMSO, 0.005 μ M IDA alone, 0.005 μ M ANA alone, 0.005 μ M IDA and 5 μ M ANA for 72 h. J Colony formation in primary cells obtained from AML patient #6 as determined via cell counting. Data are presented as the mean \pm SD (n = 3). Comparisons were evaluated using the two-tailed Student's t-test, and multiple groups were analyzed using a one-way analysis of variance. *P < 0.05, **P < 0.01, ****P < 0.001, ****P < 0.0001. NS not significant.



sequencing analysis showed that the genes related to pyroptosis such as GSDME and caspase3 showed significant changes, and the mRNA levels of inflammatory factor IL-1 β were highly upregulated (Supplementary Fig. 4A, B).

Notably, the effect of cleaved-CASP on the ANA + IDA combination treatment-induced pyroptosis was confirmed since the addition of pan-caspase inhibitor Z-VAD-FMK rescued cell viability in both HEL and MOLM-16 cells (Fig. 6I). GSDME

Fig. 6 ANA combined with IDA synergistically inhibiting the growth of high PDE3A-expressing AML cells through pyroptosis. A Volcano plots of normalized gene expression in HEL cells with or without IDA/ANA combinatorial treatment for 72 h analyzed using RNA sequencing. B KEGG analysis of these significant gene signatures from the corresponding normalized enrichment score (NES). C Heatmap of differentially expressed genes in HEL cells in the "MAPK signaling pathway" following the combination treatment with IDA and ANA. Each column represents a sample, each row represents a gene, blue represents the downregulation of genes, and red represents the upregulation of genes. D, E Significantly enriched GSEA signatures in the transcriptional profile of HEL cells following the combination treatment with IDA and ANA. The normalized enrichment score (NES) and *P*-value are shown. F The adjusted *P*-value and fold change of the related differentially expressed genes are shown in the table. G HEL and MOLM-16 cells were treated with 0.005 μM IDA alone, 1 μM ANA alone, 0.005 μM IDA and 1 μM ANA for 2 h and then subjected to western blot analysis to detect any changes in the expression of related proteins. H ELISA assay of IL-1β and IL-18 levels in supernatants from cell cultures. I A CCK-8 assay of cell viability in the HEL and MOLM-16 cell lines treated with ANA combined with IDA and the pan-caspase inhibitor Z-VAD-FMK. J, K A CCK-8 cell viability assay of the HEL and MOLM-16 cell lines infected with two independent shRNA targeting GSDME and treated with ANA combined with IDA. Data are presented as the mean ± SD (n = 3). Comparisons were evaluated using the two-tailed Student's *t*-test, and multiple groups were analyzed using a one-way analysis of variance. *P < 0.05, **P < 0.01, ****P < 0.001, *** one-way analysis of variance. *P < 0.05, **P < 0.01, ****P < 0.001, ****P < 0.001, *** one-way analysis of variance.

knockdown (Fig. 6J) reverted the synergistic effects of ANA + IDA (Fig. 6K).

In conclusion, ANA combined with IDA synergistically inhibits the growth of high PDE3A-expressing AML cells. The primary mechanism underlying this inhibition appears to be pyroptosis, which is initiated by caspase-3 activation triggering GSDME cleavage.

Combination of ANA with IDA exerting synergistic antileukemia effects on AML xenograft mouse models

We tested the efficacy of ANA and IDA combination in vivo using an AML xenograft mouse model (Fig. 7A). The result showed that the combination treatment of IDA and ANA significantly reduced the leukemia burden (Fig. 7B) and extended the survival time compared with single-drug treatment (Fig. 7C). The IDA-ANA combination-treated mice exhibited smaller and lighter livers and spleens than the other groups and controls (Fig. 7D, E, Supplementary Fig. 5A). Complete blood count revealed that besides the reduction of platelet after the treatment of ANA and IDA, other types of hemocytes remained unaffected, demonstrating the safety of the drug combination (Fig. 7F, Supplementary Fig. 5B-G). The cleaved GSDME-N in mice livers was significantly upregulated when the mice were treated with IDA and ANA compared with the expression levels of those treated with IDA or ANA alone (Fig. 7G). Congruently, evidence for this significant decrease in tumor burden was observed in the IHC analysis of anti-human CD45 cells in the liver, spleen, and bone marrow of the combination-treated mice (Fig. 7H). HE staining was also performed, and it revealed the histological decrease in HEL cell infiltration by combination treatment with IDA and ANA in the liver, spleen, and bone marrow compared with that after treatment with ANA or IDA alone (Supplementary Fig. 5H).

Collectively, these data suggest that the ANA-IDA combination has a strong anti-leukemia effect on AML cells in vivo and could reduce the severity of disease-associated hepatomegaly and splenomegaly.

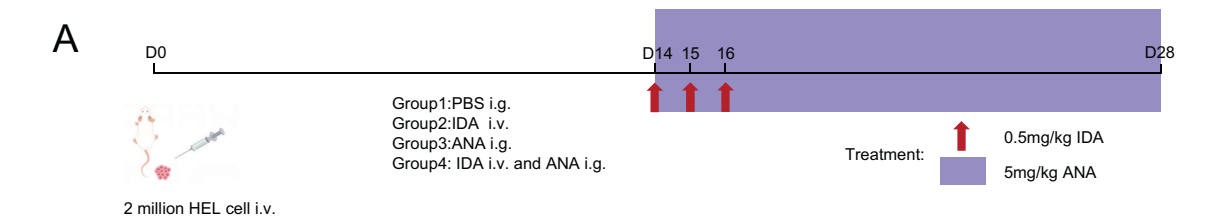
DISCUSSION

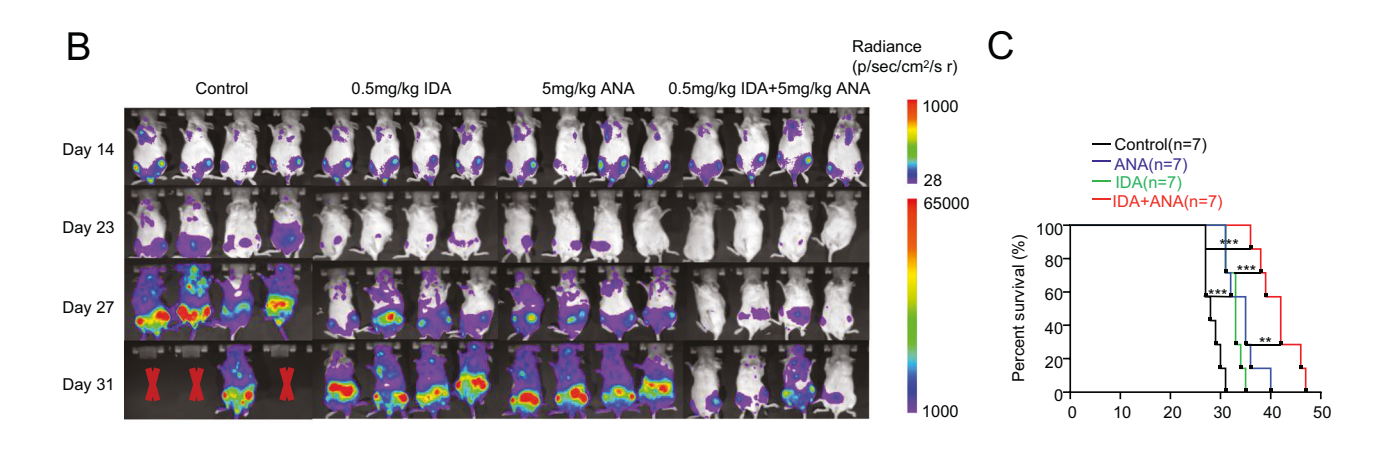
AML is a neoplastic disorder arising from hematopoietic progenitor cells. Novel therapeutic targets and interventions for AML are imperative. The pivotal discovery of our study was the identification of pronounced high PDE3A expression intricately linked to unfavorable prognostic outcomes in patients with AML. Moreover, the PDE3A inhibitor ANA effectively curtailed the growth of AML cells exhibiting high PDE3A expression in vitro and in vivo. Crucially, the downregulation of drug resistance-associated genes in AML cells after ANA treatment augmented the responsiveness of these cells to the chemotherapeutic agent IDA, a mainstay of AML treatment, both in vivo and in vitro. Consequently, the combined application of ANA and IDA holds promise as a therapeutic avenue for AML patients with elevated PDE3A expression levels.

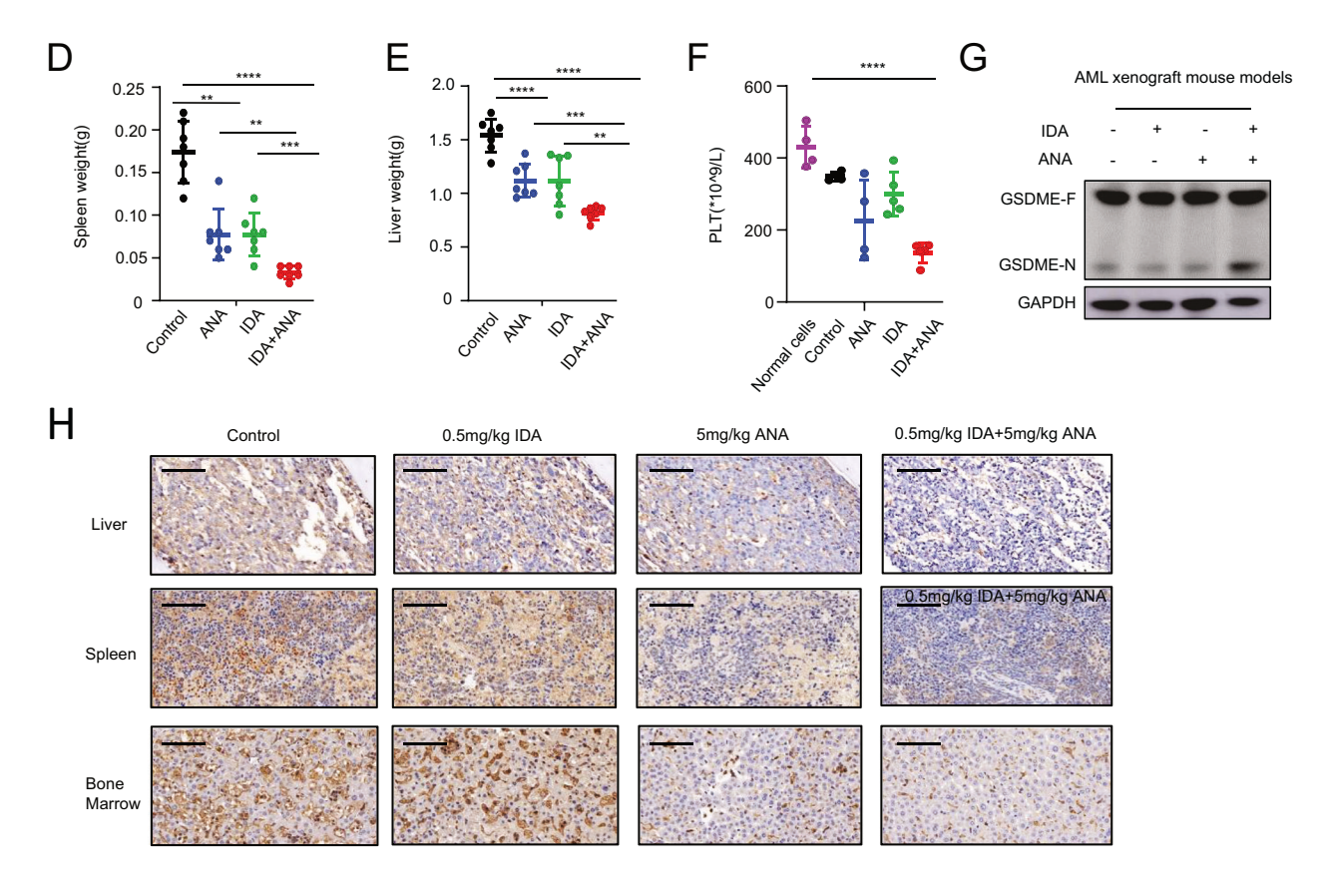
Universal overexpression of PDE3A has been documented in various cancer types, such as liver cancer, cervical carcinoma, and colon cancer [21]. However, the mechanism through which PDE3A inhibitors exert their effects hinges on the expression of SLFN12 in cancer cells. PDE3A inhibitors have negligible effects on cancer cells with low PDE3A expression [10, 24]. This variability may explain the varying sensitivities of AML cell lines to the PDE3A inhibitor ANA. Notably, recent studies have revealed that PDE3A is a core target gene of MYBL2. Attenuation of MYBL2 activity results in G2/M phase cell cycle arrest through the p53-p21-DREAM-CDE/CHR pathway in melanoma cancer cells [14]. Our findings corroborate this concept as evidenced by the time-dependent change in cell cycle-associated protein levels following ANA treatment.

ANA treatment downregulated the key drug-resistant genes such as EGR1, DUSP16, PAK1, and p-SRC. The GDNF-RET-EGR1 signaling axis is implicated in fostering drug resistance by activating Cyclin D1 [29], while the cell cycle is interrupted via G1 arrest by ANA in HEL and MOLM-16 cells. Notably, the AhR/SRC axis showed therapeutic vulnerability, prompting the consideration of SRC inhibitors as adjunctive agents, along with frontline therapies, to impede the onset of melanoma resistance [38]. Recent investigations have demonstrated that SRC activation can lead to the inhibition of downstream p38 MAPK or ERK MAPK signaling pathways in cancer cells [39] and play contributory roles in platelet adhesion and metastasis [6]. In this context, the administration of ANA has the potential to augment the drug sensitivity of therapeutic agents.

Our findings underscore the remarkable synergism between ANA and IDA, particularly in high PDE3A-expressing AML cells, among the seven anti-leukemia drugs evaluated. Our western blotting analysis revealed a plausible mechanistic pathway for the effectiveness of this combination, implicating pyroptosis as a crucial component likely mediated by the cleavage of GSDME. Studies have proposed that the MAPK signaling pathway is an upstream regulator of the caspase-3/GSDME signaling cascade [40, 41] and have introduced the novel notion that GSDME, a member of the gasdermin family, can be cleaved by active caspase-3, releasing the N-terminal effector domain. Upon exposure to chemotherapy, this domain creates pores in the cell membrane, causing cell pyroptosis [42]. The caspase-3/GSDME signaling pathway functions as a pivotal switch between apoptosis and pyroptosis in cancer cells. When GSDME is highly expressed, active caspase-3 cleaves it, liberating the N-terminal domain that punctures the cell membrane and leading to pyroptosis. Low GSDME expression led to apoptosis. Notably, caspase-8 was cleaved prior to caspase-3 in both scenarios [43], which may explain the absence of apoptosis in HEL and MOLM-16 cells treated with ANA and IDA for 72 h. Notably, the induction of pyroptosis possesses robust antitumor immune effects [44], marked by the release of proinflammatory cytokines that stimulate immune cell activation, subsequently enhancing chemosensitivity.







Our study introduces the novel perspective that pyroptosis participates in the combined treatment paradigm of ANA and IDA in AML.

In conclusion, our study represents a pioneering effort to reveal the adverse prognostic implications of elevated PDE3A expression in patients with AML. ANA demonstrated a synergistic effect when combined with IDA in vitro and in vivo. These findings substantiate the potential of a therapeutic strategy involving the integration of PDE3A inhibition with conventional chemotherapeutic agents for the treatment of AML.

Fig. 7 Combination of ANA with IDA exerting synergistic anti-leukemia effects on AML xenograft mouse model. A HEL-luci cells were injected intravenously into the NSG mice $(2 \times 10^6$ cells per mouse). Fourteen days later, the mice were treated with vehicle treatment, IDA alone (0.5 mg/kg, iv, days 14–16), ANA alone (5 mg/kg, po, days 14–28), or combination treatment as indicated. **B** Bioluminescence imaging of representative mice from each group obtained on days 14, 23, 27, and 31. **C** Survival curve of each group of mice. P-values were determined using the log-rank test (n = 7). **D** Weight of representative spleens from sacrificed mice. **E** Weight of representative livers from sacrificed mice. **F** Blood routine of experimental mice in each group. **G** The livers of NSG mice were obtained and subjected to western blot analysis to detect any changes in the expression of cleaved GSDME-N. **H** Immunohistochemical staining for hCD45 of histologic sections of the bone marrow, liver, and spleen in experimental mice. Data are presented as the mean \pm SD (n = 3). Comparisons were evaluated using the two-tailed Student's t-test, and multiple groups were analyzed using a one-way analysis of variance. *P < 0.05, **P < 0.01, ****P < 0.001, ****P < 0.0001, NS not significant.

DATA AVAILABILITY

Our sequencing and processed data files were submitted to the Gene Expression Omnibus (GEO; http://www.ncbi.nlm.nih.gov/geo/) repository GSE269021 (RNA-seq). Other relevant data are available from the corresponding authors upon reasonable request.

REFERENCES

- Döhner H, Weisdorf DJ, Bloomfield CD. Acute myeloid leukemia. N Engl J Med. 2015;373:1136–52. https://doi.org/10.1056/NEJMra1406184
- He X, Zhu Y, Lin YC, Li M, Du J, Dong H, et al. PRMT1-mediated FLT3 arginine methylation promotes maintenance of FLT3-ITD(+) acute myeloid leukemia. Blood. 2019;134:548–60. https://doi.org/10.1182/blood.2019001282
- 3. Rubnitz JE, Kaspers GJL. How I treat pediatric acute myeloid leukemia. Blood. 2021;138:1009–18. https://doi.org/10.1182/blood.2021011694
- Pui CH, Mullighan CG, Evans WE, Relling MV. Pediatric acute lymphoblastic leukemia: where are we going and how do we get there? Blood. 2012;120:1165–74. https://doi.org/10.1182/blood-2012-05-378943
- Mezouar S, Darbousset R, Dignat-George F, Panicot-Dubois L, Dubois C. Inhibition
 of platelet activation prevents the P-selectin and integrin-dependent accumulation of cancer cell microparticles and reduces tumor growth and metastasis
 in vivo. Int J Cancer. 2015;136:462–75. https://doi.org/10.1002/ijc.28997
- Zhang X, Xu H, Bi X, Hou G, Liu A, Zhao Y, et al. Src acts as the target of matrine to inhibit the proliferation of cancer cells by regulating phosphorylation signaling pathways. Cell Death Dis. 2021;12:931. https://doi.org/10.1038/s41419-021-04221-6
- Foss B, Bruserud O. Platelet functions and clinical effects in acute myelogenous leukemia. Thromb Haemost. 2008;99:27–37. https://doi.org/10.1160/TH07-04-0240
- Cacic D, Nordgård O, Meyer P, Hervig T. Platelet microparticles decrease daunorubicin-induced DNA damage and modulate intrinsic apoptosis in THP-1 cells. Int J Mol Sci. 2021;22:7264. https://doi.org/10.3390/ijms22147264
- Zhang W, Colman RW. Thrombin regulates intracellular cyclic AMP concentration in human platelets through phosphorylation/activation of phosphodiesterase 3A. Blood. 2007;110:1475–82. https://doi.org/10.1182/blood-2006-10-052522
- An R, Liu J, He J, Wang F, Zhang Q, Yu Q. PDE3A inhibitor anagrelide activates death signaling pathway genes and synergizes with cell death-inducing cytokines to selectively inhibit cancer cell growth. Am J Cancer Res. 2019;9:1905–21.
- Colman RW. Platelet cyclic adenosine monophosphate phosphodiesterases: targets for regulating platelet-related thrombosis. Semin Thromb Hemost. 2004;30:451–60. https://doi.org/10.1055/s-2004-833480
- Yan B, Ding Z, Zhang W, Cai G, Han H, Ma Y, et al. Multiple PDE3A modulators act as molecular glues promoting PDE3A-SLFN12 interaction and induce SLFN12 dephosphorylation and cell death. Cell Chem Biol. 2022;29:958–69.e5. https:// doi.org/10.1016/j.chembiol.2022.01.006
- Hao N, Shen W, Du R, Jiang S, Zhu J, Chen Y, et al. Phosphodiesterase 3A represents a therapeutic target that drives stem cell-like property and metastasis in breast cancer. Mol Cancer Ther. 2020;19:868–81. https://doi.org/10.1158/1535-7163.MCT-18-1233
- Zhong F, Liu J, Gao C, Chen T, Li B. Downstream regulatory network of MYBL2 mediating its oncogenic role in melanoma. Front Oncol. 2022;12:816070. https://doi.org/10.3389/fonc.2022.816070
- Tian FM, Zhong CY, Wang XN, Meng Y. PDE3A is hypermethylated in cisplatin resistant non-small cell lung cancer cells and is a modulator of chemotherapy response. Eur Rev Med Pharm Sci. 2017;21:2635–41.
- Storen EC, Tefferi A. Long-term use of anagrelide in young patients with essential thrombocythemia. Blood. 2001;97:863–6. https://doi.org/10.1182/blood.v97.4.863
- Tomer A. Effects of anagrelide on in vivo megakaryocyte proliferation and maturation in essential thrombocythemia. Blood. 2002;99:1602–9. https://doi.org/ 10.1182/blood.v99.5.1602
- Pulkka OP, Gebreyohannes YK, Wozniak A, Mpindi JP, Tynninen O, Icay K, et al. Anagrelide for gastrointestinal stromal tumor. Clin Cancer Res. 2019;25:1676–87. https://doi.org/10.1158/1078-0432.CCR-18-0815

- Chen J, Liu N, Huang Y, Wang Y, Sun Y, Wu Q, et al. Structure of PDE3A-SLFN12 complex and structure-based design for a potent apoptosis inducer of tumor cells. Nat Commun. 2021;12:6204. https://doi.org/10.1038/s41467-021-26546-8
- Meanwell NA. Anagrelide: a clinically effective cAMP phosphodiesterase 3A inhibitor with molecular glue properties. ACS Med Chem Lett. 2023;14:350–61. https://doi.org/10.1021/acsmedchemlett.3c00092
- de Waal L, Lewis TA, Rees MG, Tsherniak A, Wu X, Choi PS, et al. Identification of cancer-cytotoxic modulators of PDE3A by predictive chemogenomics. Nat Chem Biol. 2016;12:102–8. https://doi.org/10.1038/nchembio.1984
- Garvie CW, Wu X, Papanastasiou M, Lee S, Fuller J, Schnitzler GR, et al. Structure of PDE3A-SLFN12 complex reveals requirements for activation of SLFN12 RNase. Nat Commun. 2021;12:4375. https://doi.org/10.1038/s41467-021-24495-w
- Wu X, Schnitzler GR, Gao GF, Diamond B, Baker AR, Kaplan B, et al. Mechanistic insights into cancer cell killing through interaction of phosphodiesterase 3A and schlafen family member 12. J Biol Chem. 2020;295:3431–46. https://doi.org/ 10.1074/jbc.RA119.011191
- Li D, Chen J, Ai Y, Wang Y, Sun Y, Wu Q, et al. Estrogen-related hormones induce apoptosis by stabilizing Schlafen-12 protein turnover. Mol Cell. 2019;75:1103–16.e9. https://doi.org/10.1016/j.molcel.2019.06.040
- Ai Y, He H, Chen P, Yan B, Zhang W, Ding Z, et al. An alkaloid initiates phosphodiesterase 3A-schlafen 12 dependent apoptosis without affecting the phosphodiesterase activity. Nat Commun. 2020;11:3236. https://doi.org/10.1038/s41467-020-17052-4
- Dos Santos C, McDonald T, Ho YW, Liu H, Lin A, Forman SJ, et al. The Src and c-Kit kinase inhibitor dasatinib enhances p53-mediated targeting of human acute myeloid leukemia stem cells by chemotherapeutic agents. Blood. 2013;122:1900–13. https://doi.org/10.1182/blood-2012-11-466425
- Liu J, Ren G, Li K, Liu Z, Wang Y, Chen T, et al. The Smad4-MYO18A-PP1A complex regulates β-catenin phosphorylation and pemigatinib resistance by inhibiting PAK1 in cholangiocarcinoma. Cell Death Differ. 2022;29:818–31. https://doi.org/ 10.1038/s41418-021-00897-7
- Low HB, Wong ZL, Wu B, Kong LR, Png CW, Cho YL, et al. DUSP16 promotes cancer chemoresistance through regulation of mitochondria-mediated cell death. Nat Commun. 2021;12:2284. https://doi.org/10.1038/s41467-021-22638-7
- Marks BA, Pipia IM, Mukai C, Horibata S, Rice EJ, Danko CG, et al. GDNF-RET signaling and EGR1 form a positive feedback loop that promotes tamoxifen resistance via cyclin D1. BMC Cancer. 2023;23:138. https://doi.org/10.1186/s12885-023-10559-1
- Liu Y, Kimpara S, Hoang NM, Daenthanasanmak A, Li Y, Lu L, et al. EGR1-mediated metabolic reprogramming to oxidative phosphorylation contributes to ibrutinib resistance in B-cell lymphoma. Blood. 2023;142:1879–94.
- 31. Ren Q, Guo F, Tao S, Huang R, Ma L, Fu P. Flavonoid fisetin alleviates kidney inflammation and apoptosis via inhibiting Src-mediated NF-κB p65 and MAPK signaling pathways in septic AKI mice. Biomed Pharmacother. 2020;122:109772. https://doi.org/10.1016/i.biopha.2019.109772
- 32. Yang S, Li F, Lu S, Ren L, Bian S, Liu M, et al. Ginseng root extract attenuates inflammation by inhibiting the MAPK/NF-κB signaling pathway and activating autophagy and p62-Nrf2-Keap1 signaling in vitro and in vivo. J Ethnopharmacol. 2022;283:114739. https://doi.org/10.1016/j.jep.2021.114739
- Cao Y, Chen J, Ren G, Zhang Y, Tan X, Yang L. Punicalagin prevents inflammation in LPS-induced RAW264.7 macrophages by inhibiting FoxO3a/Autophagy signaling pathway. Nutrients. 2019;11:2794. https://doi.org/10.3390/nu11112794
- Yu P, Zhang X, Liu N, Tang L, Peng C, Chen X. Pyroptosis: mechanisms and diseases.
 Signal Transduct Target Ther. 2021;6:128. https://doi.org/10.1038/s41392-021-00507-5
- Bertheloot D, Latz E, Franklin BS. Necroptosis, pyroptosis and apoptosis: an intricate game of cell death. Cell Mol Immunol. 2021;18:1106–21. https://doi.org/ 10.1038/s41423-020-00630-3
- Huang Y, Xu W, Zhou R. NLRP3 inflammasome activation and cell death. Cell Mol Immunol. 2021;18:2114–27. https://doi.org/10.1038/s41423-021-00740-6
- Wang Y, Kanneganti TD. From pyroptosis, apoptosis and necroptosis to panoptosis: a mechanistic compendium of programmed cell death pathways. Comput Struct Biotechnol J. 2021;19:4641–57. https://doi.org/10.1016/j.csbj.2021.07.038

- Paris A, Tardif N, Baietti FM, Berra C, Leclair HM, Leucci E, et al. The AhR-SRC axis as a therapeutic vulnerability in BRAFi-resistant melanoma. EMBO Mol Med. 2022;14:e15677. https://doi.org/10.15252/emmm.202215677
- Jin AL, Zhang CY, Zheng WJ, Xian JR, Yang WJ, Liu T, et al. CD155/SRC complex promotes hepatocellular carcinoma progression via inhibiting the p38 MAPK signalling pathway and correlates with poor prognosis. Clin Transl Med. 2022;12:e794. https://doi.org/10.1002/ctm2.794
- Peng Z, Wang P, Song W, Yao Q, Li Y, Liu L, et al. GSDME enhances cisplatin sensitivity to regress non-small cell lung carcinoma by mediating pyroptosis to trigger antitumor immunocyte infiltration. Signal Transduct Target Ther. 2020;5:159. https://doi.org/10.1038/s41392-020-00274-9
- Ren J, Tao Y, Peng M, Xiao Q, Jing Y, Huang J, et al. Targeted activation of GPER enhances the efficacy of venetoclax by boosting leukemic pyroptosis and CD8+ T cell immune function in acute myeloid leukemia. Cell Death Dis. 2022;13:915. https://doi.org/10.1038/s41419-022-05357-9
- Wang Y, Gao W, Shi X, Ding J, Liu W, He H, et al. Chemotherapy drugs induce pyroptosis through caspase-3 cleavage of a gasdermin. Nature. 2017;547:99–103. https://doi.org/10.1038/nature22393
- 43. Jiang M, Qi L, Li L, Li Y. The caspase-3/GSDME signal pathway as a switch between apoptosis and pyroptosis in cancer. Cell Death Discov. 2020;6:112. https://doi.org/10.1038/s41420-020-00349-0
- Zhang Z, Zhang Y, Xia S, Kong Q, Li S, Liu X, et al. Gasdermin E suppresses tumour growth by activating anti-tumour immunity. Nature. 2020;579:415–20. https:// doi.org/10.1038/s41586-020-2071-9

ACKNOWLEDGEMENTS

We thank the editor, April Jade, servicing at www.editage.cn who provided a deep revision of the manuscript.

AUTHOR CONTRIBUTIONS

C.Y., X.H., and Y.T. conceived the study and analyzed data; C.Y. and Z.L. performed RNA-seq; C.Y. and M.L. performed the western blotting procedure; C.Y. and R.Z. performed animal studies; S.H., C.Y., J.L., L.G., Y.Z., H.L., Y.D., and Q.J. provided clinical AML samples and collected patient information; L.G., and C.Y. conceived the experiments, S.H., Y.T., J.P., and J.L. helped organize the paper and conceived the experiments, C.Y., Y.T., P.X. S.H., and S.H. designed the study and wrote the manuscript.

FUNDING

This study was supported by the following grants: The National Key Research and Development Program of China (no. 2022YFC2502700), Jiangsu Key project,

BE2021654 to Shaoyan Hu, the National Natural Science Foundation of China (NSFC 82100229 to Yuanyuan Tian, 82200177 to Li Gao, 82170218, and 81970163 to Shaoyan Hu, 31830051 and 32370810 to Sudan He), and Suzhou Projects (GSWS2020039, 2020ZKPB02 to Shaoyan Hu, GSWS 2023048 to Yixin Hu), and the Suzhou Municipal Key Laboratory (SZS201615,SZS2023014 to Shaoyan Hu, SZS2022005 to Sudan He), and the Chinese Academy of Medical Sciences (CAMS) Innovation Fund for Medical Sciences (2022-I2M-2-004, 2021-I2M-1-041, 2021-I2M-1-047, and 2021-I2M-1-061), and the NCTIB Fund for R&D platform for Cell and Gene Therapy.

COMPETING INTERESTS

The authors declare no competing interests.

ETHICS APPROVAL AND CONSENT TO PARTICIPATE

Patient: This study was approved by the Ethics Committee of the Children's Hospital of Soochow University (No. 2017047-3) and was in accordance with Declaration of Helsinki. Informed consent was obtained from the parents or legal guardians and participants. Animal: All animal experiments were conducted in compliance with the animal care guidelines approved by the Institutional Laboratory Animal Care and Use Committee of Soochow University (SUDA20230802A05) and were in accordance with the ARRIVE guidelines.

ADDITIONAL INFORMATION

Supplementary information The online version contains supplementary material available at https://doi.org/10.1038/s41375-024-02437-x.

Correspondence and requests for materials should be addressed to Yuanyuan Tian, Sudan He, Jing Ling or Shaoyan Hu.

Reprints and permission information is available at http://www.nature.com/

Publisher's note Springer Nature remains neutral with regard to jurisdictional claims in published maps and institutional affiliations.

Springer Nature or its licensor (e.g. a society or other partner) holds exclusive rights to this article under a publishing agreement with the author(s) or other rightsholder(s); author self-archiving of the accepted manuscript version of this article is solely governed by the terms of such publishing agreement and applicable law.